Electronic Supplementary Information

# High throughput production of single-wall carbon nanotube fibres independent of sulfur-source

Adarsh Kaniyoor,[†a] John Bulmer, [†b] Thurid Gspann,[a] Jenifer Mizen,[a] James Ryley,[b] Patrick Kiley,[a] Jeronimo Terrones,[a] Cesar Miranda-Reyes,[a] Giorgio Divitini,[a] Martin Sparkes,[b] Bill O'Neill,[a] Alan Windle,[a] and James A. Elliott[*a]

a. Department of Materials Science and Metallurgy, 27 Charles Babbage Road, University of Cambridge, Cambridge, CB3 0FS, United Kingdom. E-mail: jae1001@cam.ac.uk
b. Institute for Manufacturing, 17 Charles Babbage Road, University of Cambridge, Cambridge, CB3 0FS, United Kingdom.

† Both authors contributed equally to this work.

S1. Precursor recipes

CNT fibres were produced using different sulfur sources, while using benzyl alcohol and ferrocene as the carbon and iron sources, respectively. The elemental ratios in the precursor feedstock are given in Table S1 below.

**Table S1**. Molar ratios of elements in the precursor solutions, calculated assuming complete dissociation inside the reactor. The carbon and iron sources are benzyl alcohol and ferrocene, respectively.

| Sulfur source | Number | Recipe | C:S | S:Fe | C:Fe |
|---|---|---|---|---|---|
| Thiophene | 1 | Low-S | 362.7 | 0.76 | 276.6 |
| | 2 | High-S | 152.2 | 1.52 | 229.1 |
| Carbon disulfide | 3 | Low-S | 362.8 | 0.76 | 276.5 |
| | 4 | High-S | 151.3 | 1.52 | 229.5 |
| Elemental sulfur | 5 | Low-S | 362.4 | 0.76 | 276.5 |

S2. Raman spectra of low S:Fe (~ 0.76) thiophene-based CNT fibres

In this section we discuss the Raman spectra of CNT fibres produced using thiophene as the sulfur source, in detail. The precursor mixture was based on recipe 1 as described in Table S1.
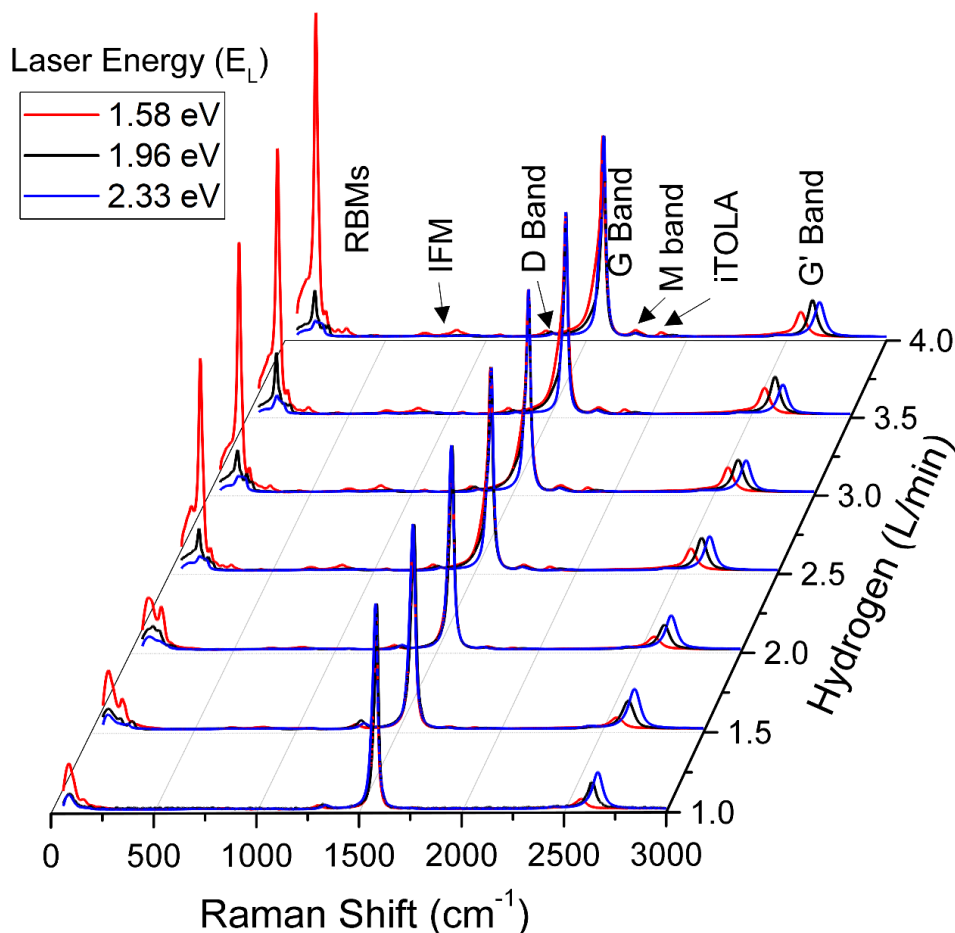


**Figure S1**. Raman spectra of CNT fibres obtained with three laser wavelengths as indicated. This Figure is same as the one presented in Figure 1(a) except that the abscissa is not truncated, allowing the IFM, M and iTOLA bands to be shown here for completeness.

S2.1. Analyses of Radial Breathing Modes (RBMs)

Representative Lorentzian fits to the Raman spectra are shown in Figure S2. Given the low resolution of the scans and the fact that bundled nanotube fibres have broad RBMs, it is difficult to fit narrow Lorentzians (of widths $3 - 5$ cm$^{-1}$) corresponding to each individual helicity that would be present. Rather, each Lorentzian here can be thought of as made up of the sum of narrower peaks, corresponding to a $2n + m$ family of tubes with the same metallicity.
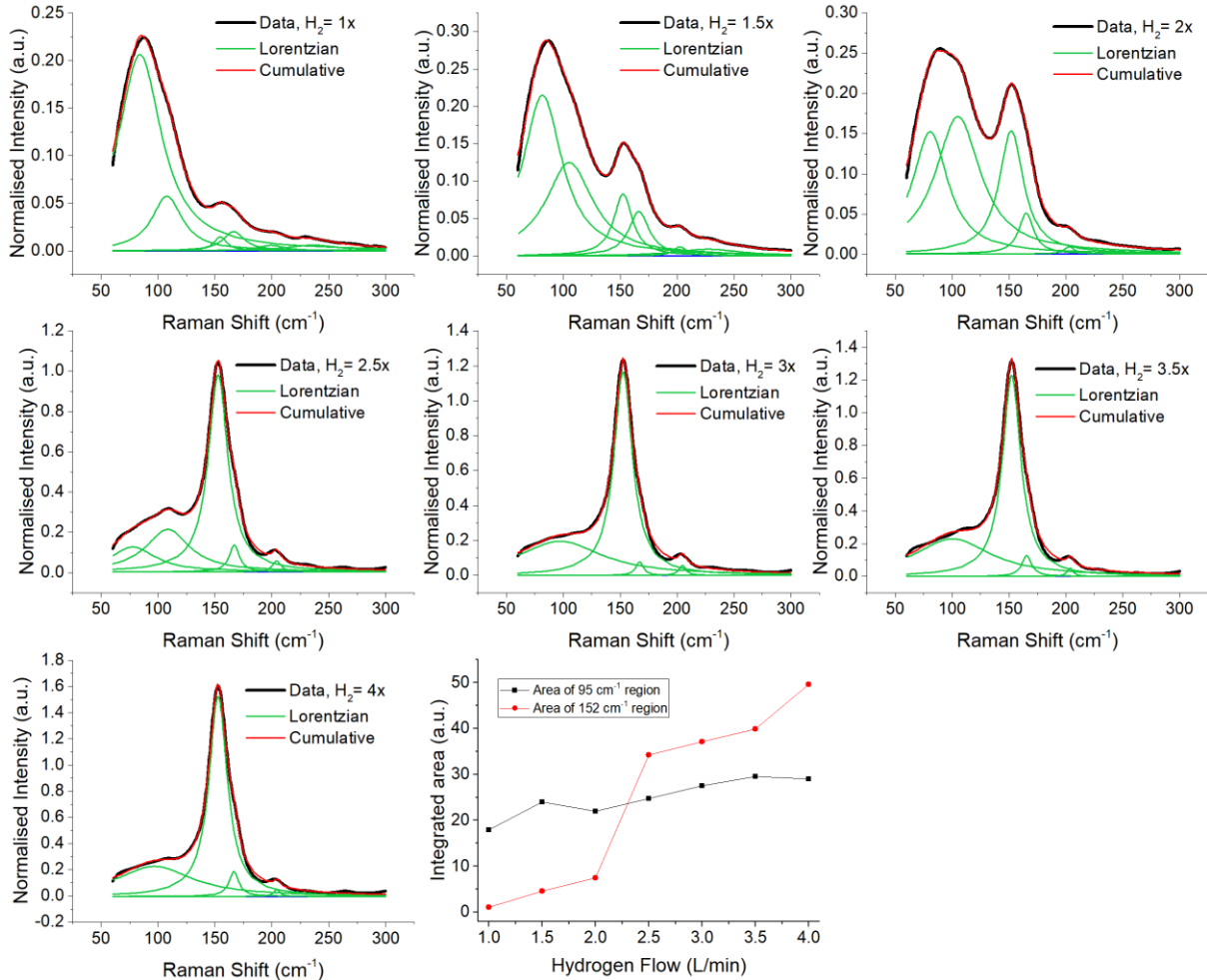
**Figure S2**. Lorentzian fits to the RBM region at $E_L$ = 1.58 eV for samples grown at different flow rates ($x$ = L min$^{-1}$). Also plotted in the last graph are the integrated area of 95 and 152 cm$^{-1}$ (including 166 cm$^{-1}$ peak) RBM regions. Note the increasing ordinate margins.

S2.2. Analyses of G band

We present here detailed analyses of the Raman G band of samples spun at increasing $H_2$ flow rates using thiophene as the sulfur source (S:Fe = 0.76). Data from three laser energies are analysed: $E_L$ = 2.33 eV in Figure S3, 1.96 eV in Figure S4, and 1.58 eV, where we consider both a three-peak (Figure S5) and a two-peak fit (Figure S6). It is usual practice to fit only two peaks to the G band but in cases where there is a likelihood of a second distribution of nanotube diameters, as is common with FC-CVD, it is possible to fit a third peak (or a second G$^-$ peak). Both at 1.96 eV and 1.58 eV, there are RBMs around 200 cm$^{-1}$ which are likely responsible for the second G$^-$ peak. The fitting methodology is explained in the methods section of the main text. The following should be noted when reading these graphs: 1) the type of G$^-$ peaks indicate metallicity with Lorentzian being semiconducting and BWF being metallic. 2) A BWF peak with an asymmetry factor, |1/q|, less than 0.07 is effectively a Lorentzian.

3
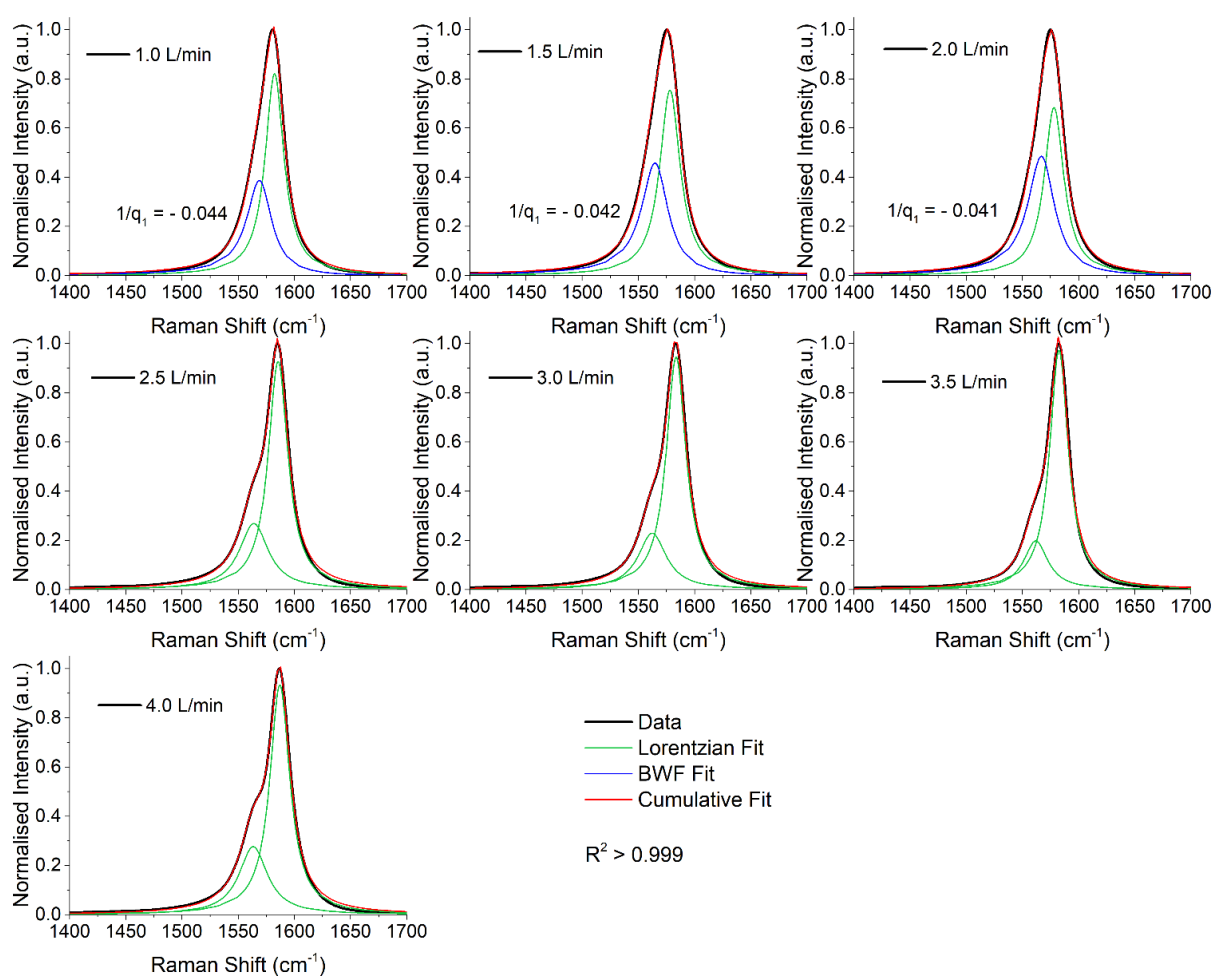
**Figure S3**. Peak fitting to G band obtained with $E_L$= 2.33 eV (532 nm) from samples grown at different hydrogen flow rates as indicated in the respective legends.

Note, that for the peak fitting in Figure S4, nearly identical fits are obtained with BWF + Lorentzian or Lorentzian + BWF fit combinations for the two $G^-$ bands, so it is difficult to assign metallicities to the two $G^-$ peaks. Since the main RBMs at this wavelength are the semiconducting 147 cm$^{-1}$ and metallic 195 cm$^{-1}$ peaks, the fitting combination presented here was considered as more appropriate. For the G band at $E_L$=1.58 eV, both the conventional two-peak ($R^2$ > 0.998) and a three-peak fitting ($R^2$ > 0.999) work well, although the three-peak fit has a better shape matching on careful observation.
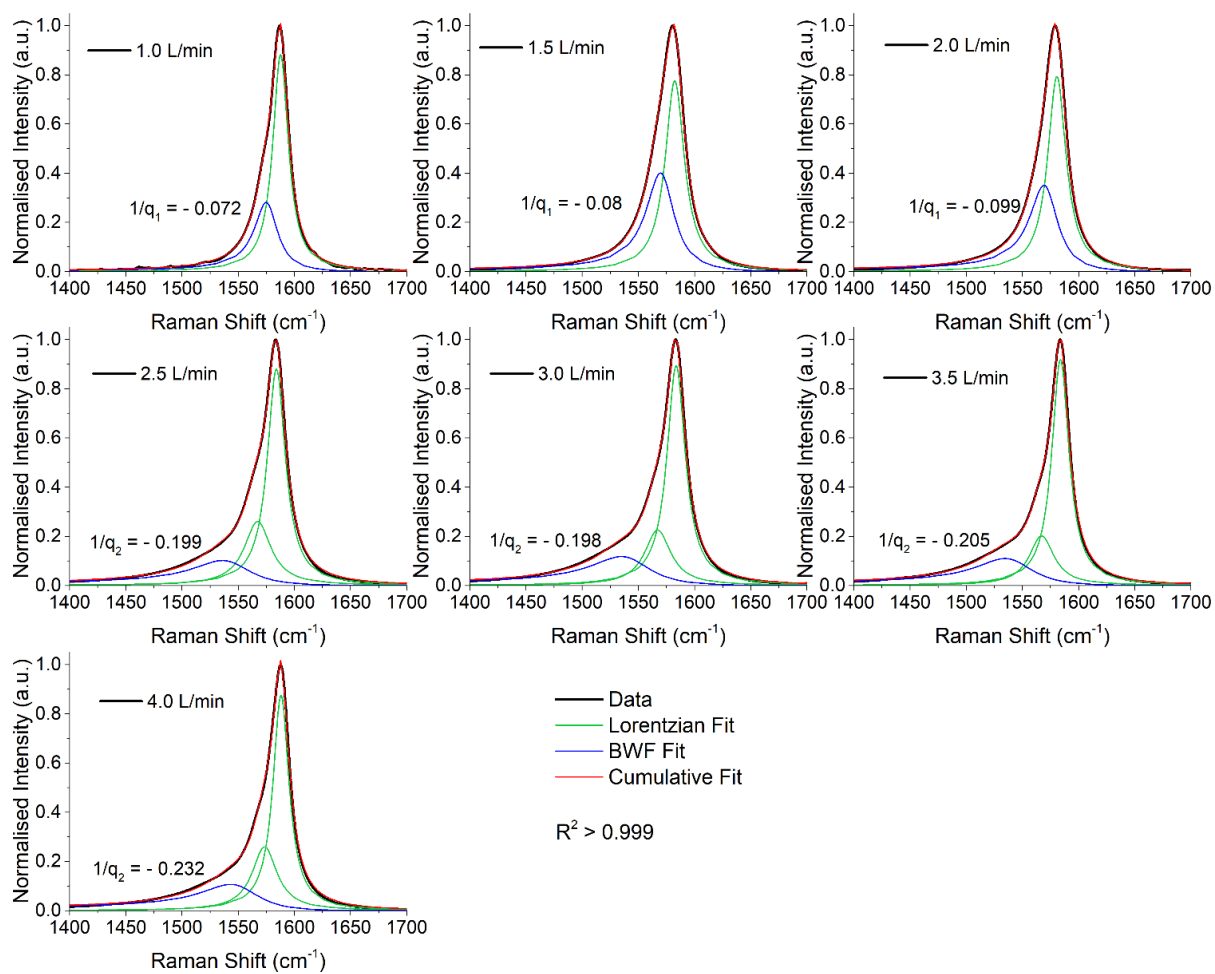
**Figure S4**. Peak fitting to G band obtained with $E_L$= 1.96 eV (633 nm) from samples grown at different hydrogen flow rates as indicated in the respective legends.
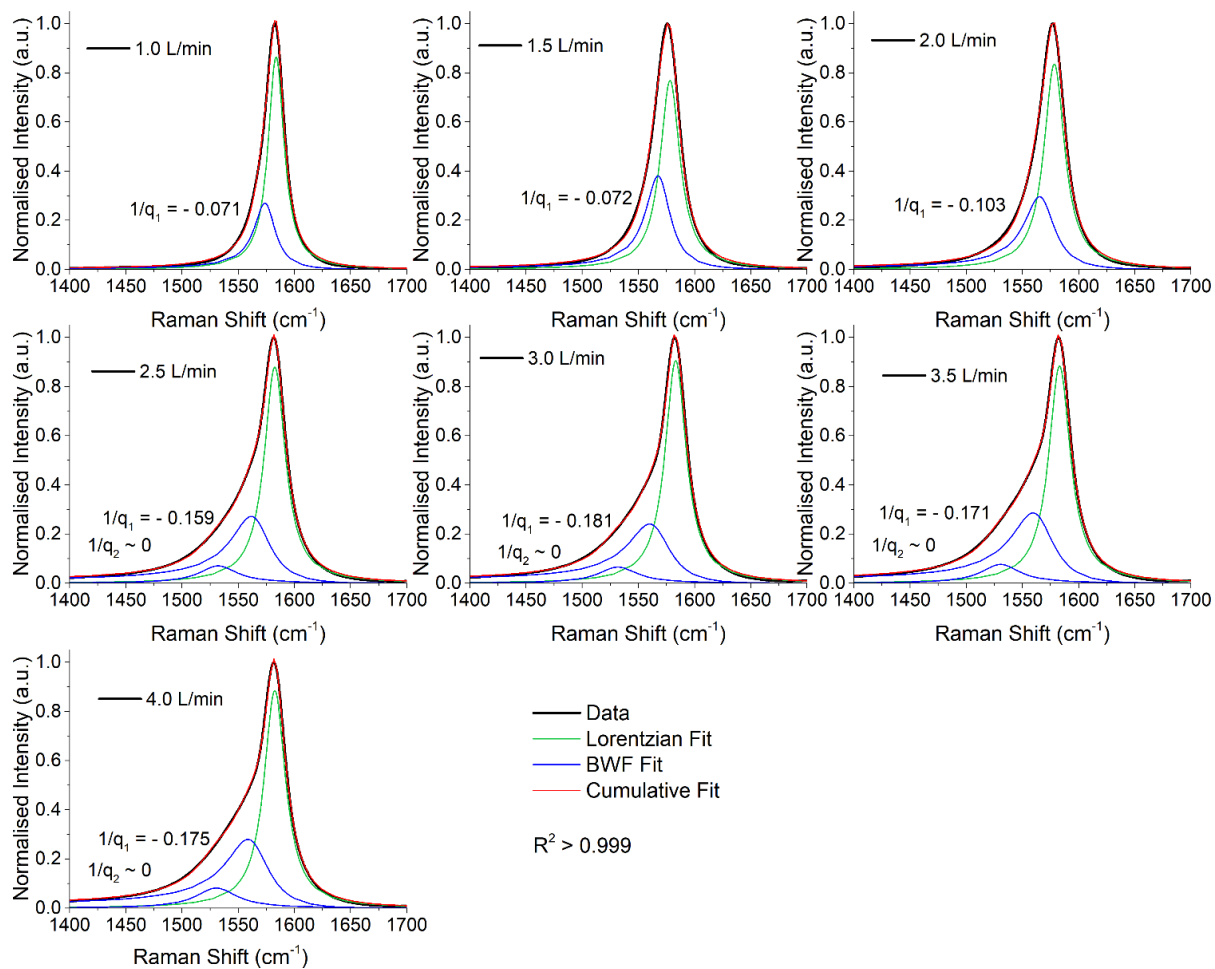
**Figure S5**. Peak fitting to G band (three-peak fit) obtained with $E_L$= 1.58 eV (785 nm) from samples grown at different hydrogen flow rates as indicated in the respective legends.
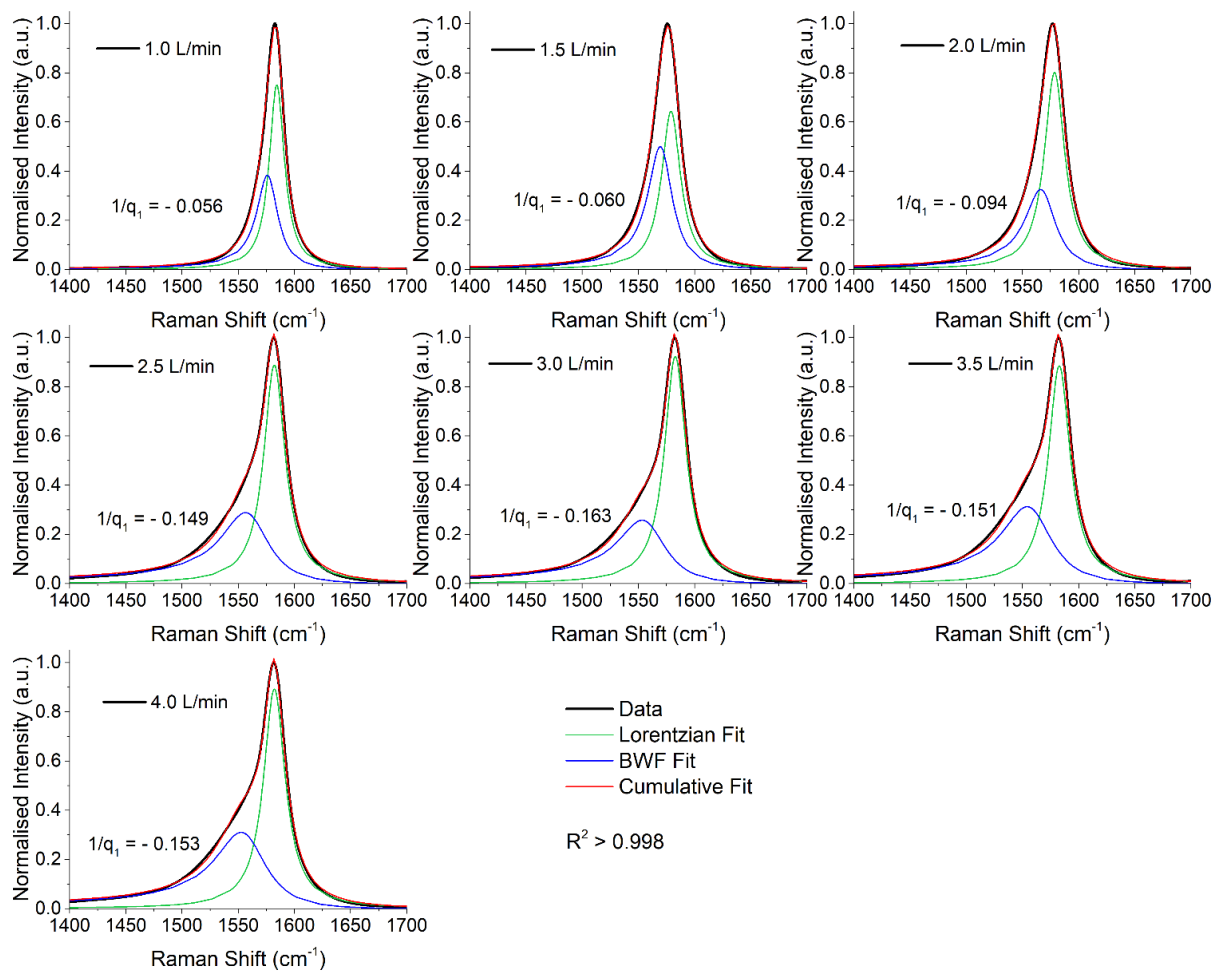
**Figure S6**. Peak fitting (two-peak fit) to G band obtained with $E_L$= 1.58 eV (785 nm) from samples grown at different hydrogen flow rates as indicated in the respective legends.

S3. Raman spectra of CNT fibres from different sulfur sources (low S:Fe)

Here, we compare the Raman spectra of fibres produced from three different sulfur sources, carbon disulfide ($CS_2$), elemental sulfur (S) and thiophene ($C_4H_4S$). Low-sulfur recipes 1,3 and 5 (see Table S1) were used as precursor mixtures. All other experimental conditions, including the reactor and feed line temperatures, were kept constant.
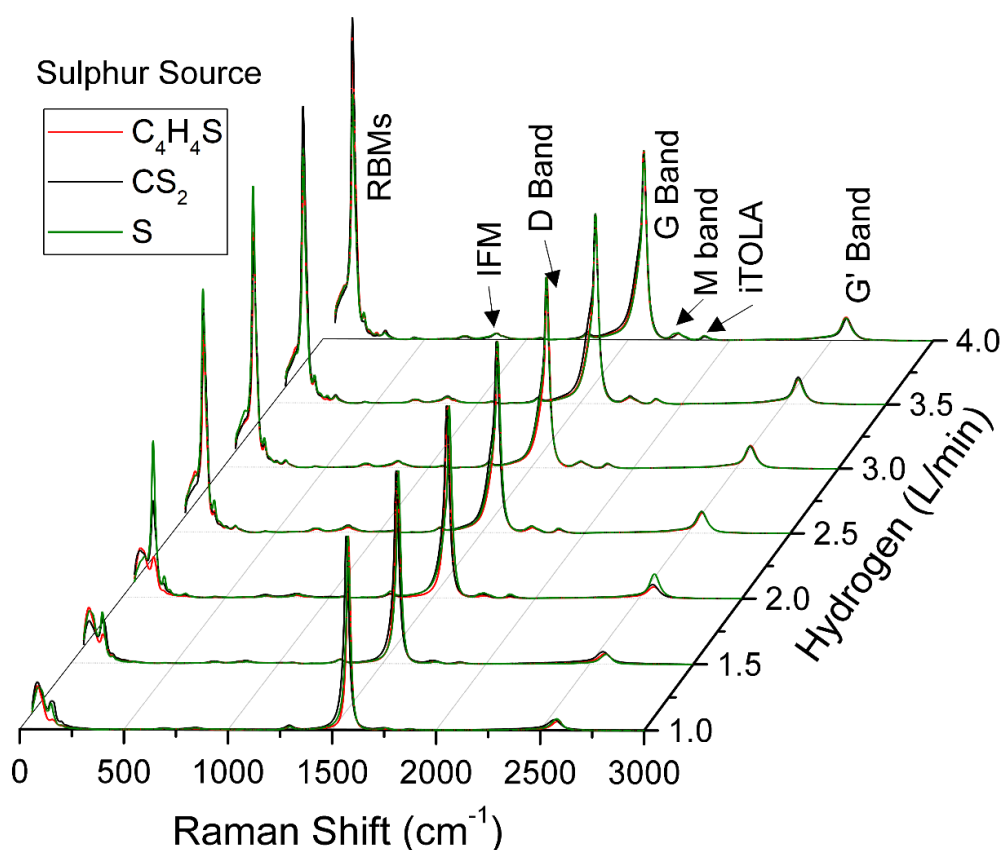


**Figure S7.** Raman spectra ($E_L$ = 1.58 eV) of CNT fibres obtained with three different sulfur sources. This Figure is equivalent to the one presented in Figure 2 (main text) but with an extended abscissa allowing IFM, M and iTOLA bands to be seen in all the cases.
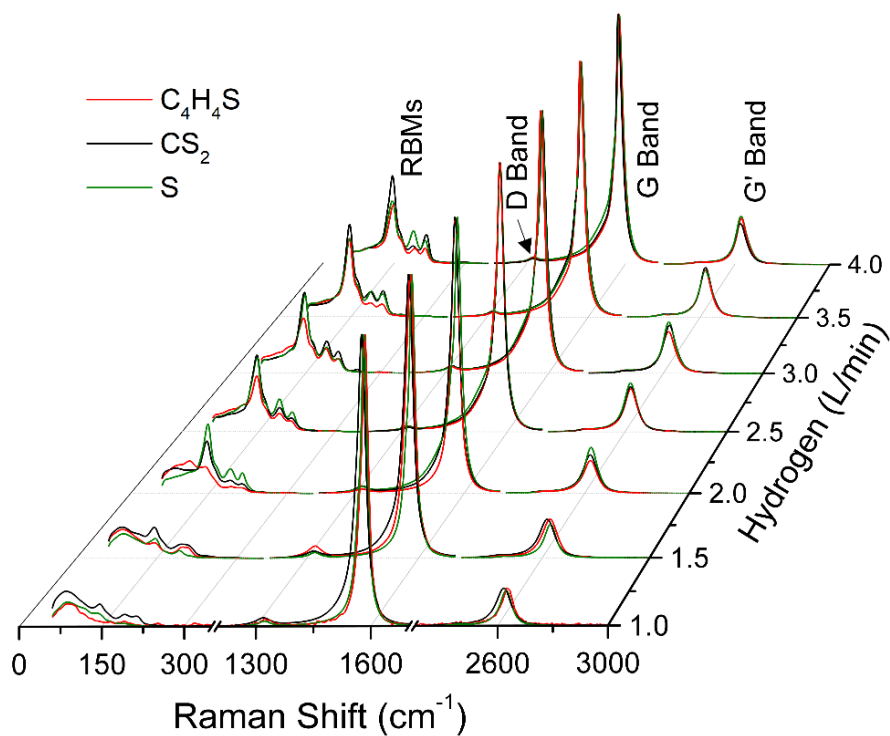
**Figure S8.** Raman spectra obtained with $E_L = 1.96$ eV of CNT fibres produced using three different sulfur sources, as indicated.
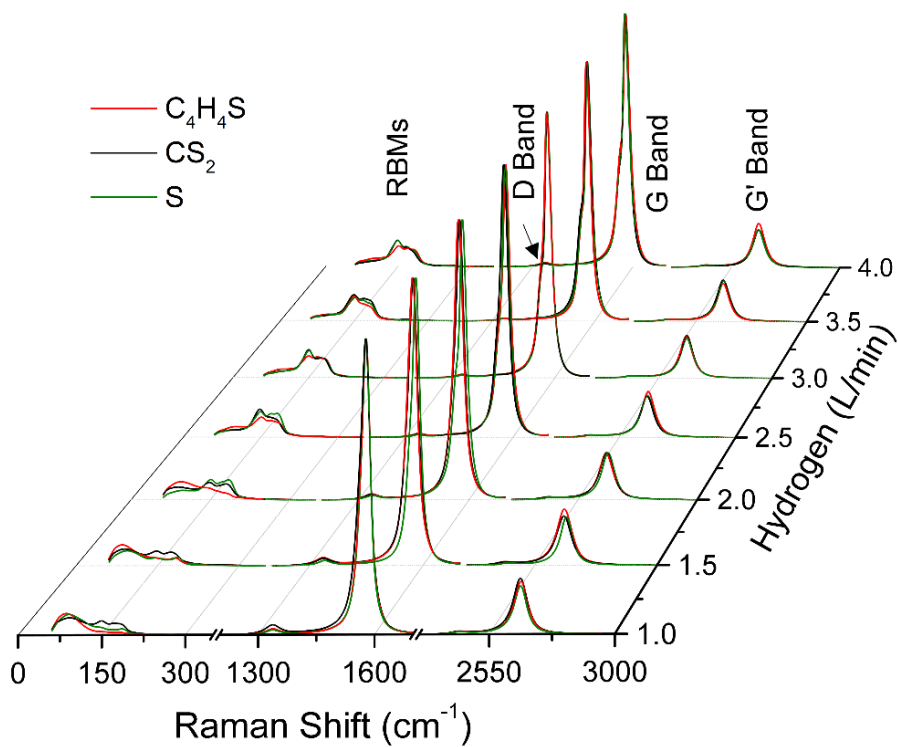


**Figure S9.** Raman spectra obtained with $E_L = 2.33$ eV of CNT fibres produced using three different sulfur sources, as indicated.

S3.1 G band deconvolution for $CS_2$ based 'low S:Fe' CNT fibres

Similar to the G band analyses for thiophene based CNT fibres, here we present the fitting analyses for carbon disulfide-based fibres. The sulfur concentrations were low and comparable to that of thiophene recipe. Notice the G band asymmetry values are higher than in thiophene samples.
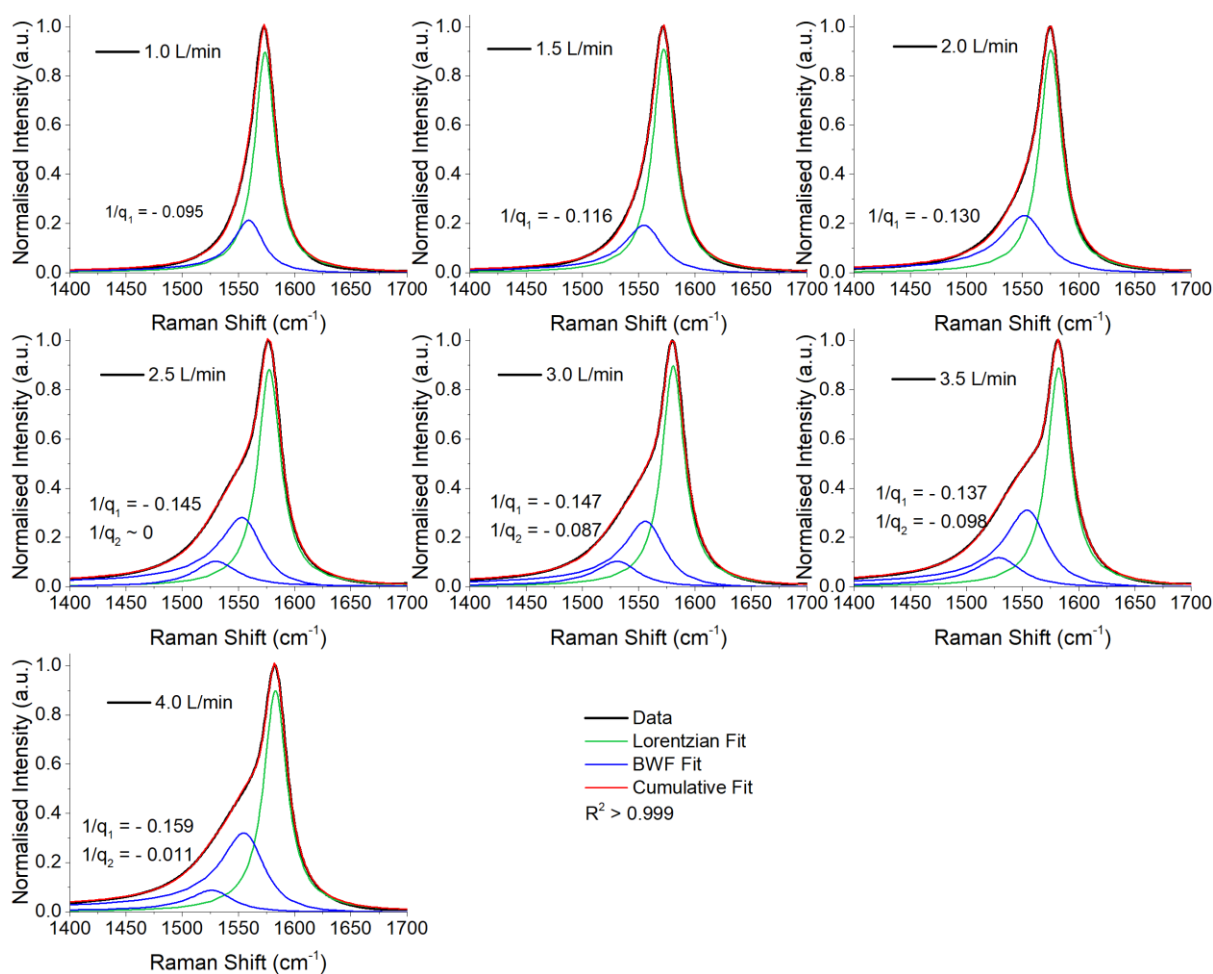


**Figure S10.** Peak fitting to G band (three-peak fit) obtained with $E_L$= 1.58 eV (785 nm) from samples grown at different hydrogen flow rates (in L min$^{-1}$) as indicated in the respective legends.
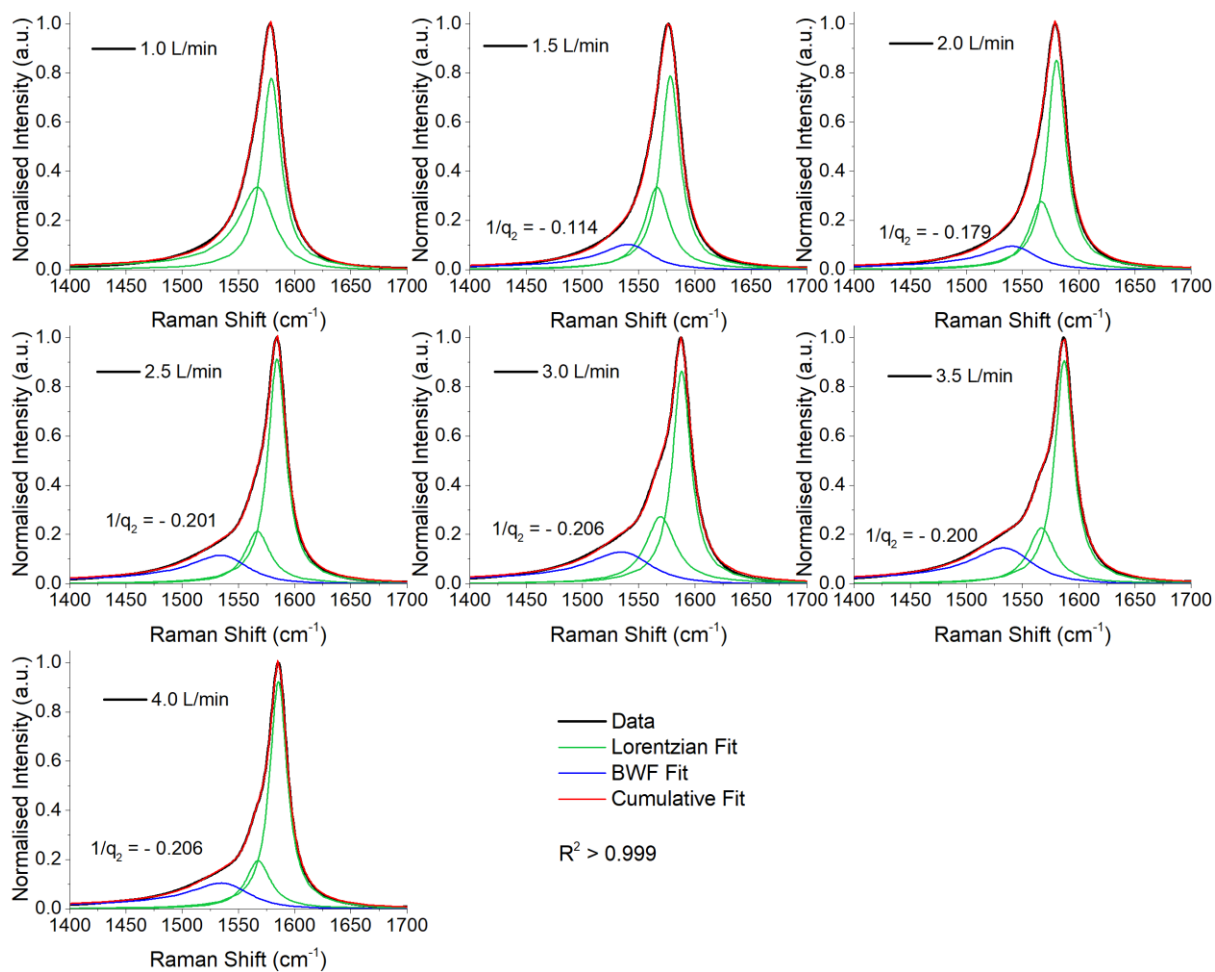
**Figure S11.** Peak fitting to G band obtained with $E_L$= 1.96 eV (633 nm) from samples grown at different hydrogen flow rates (in L min$^{-1}$) as indicated in the respective legends.
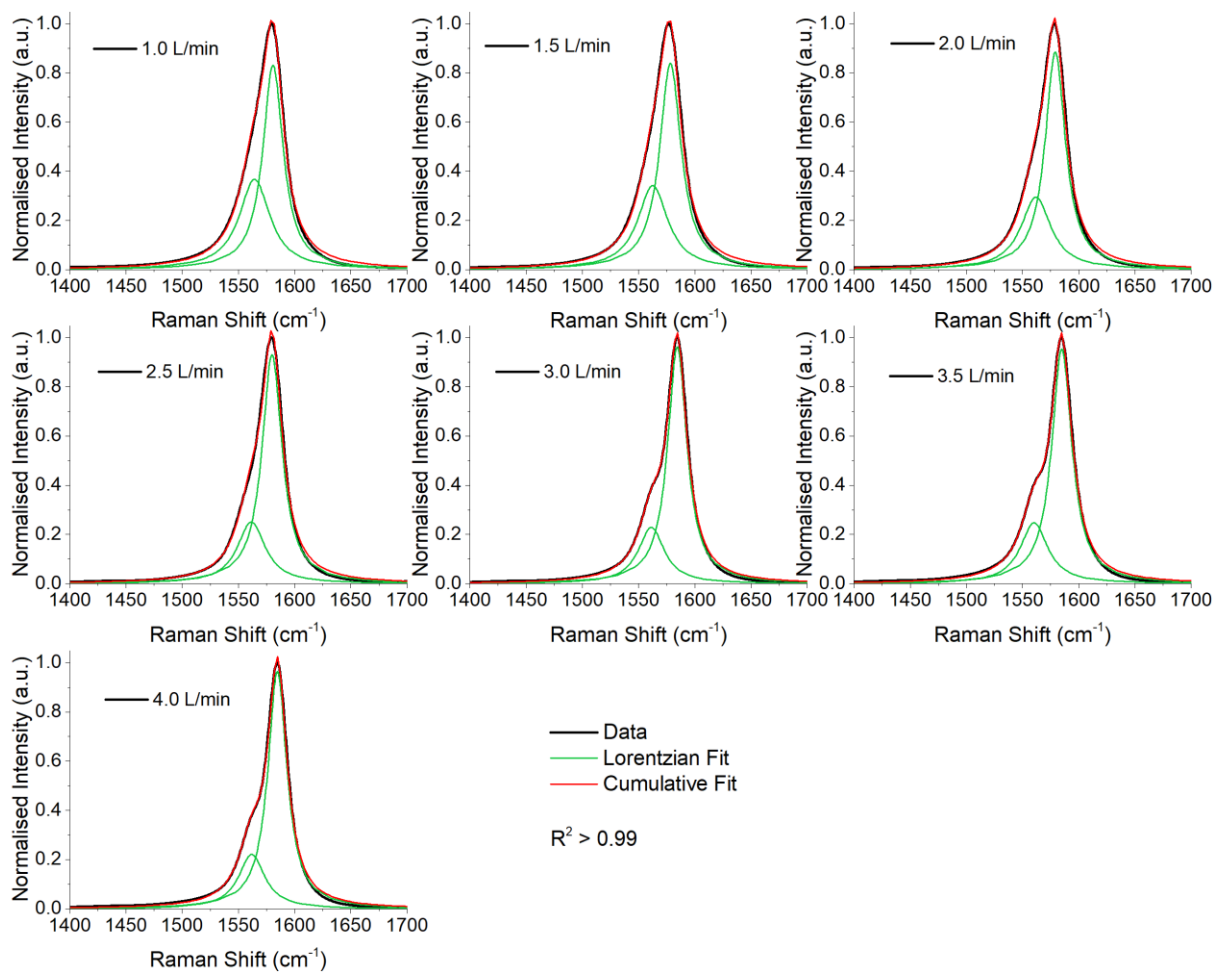
**Figure S12.** Peak fitting to G band obtained with $E_L$= 2.33 eV (532 nm) from samples grown at different hydrogen flow rates (in L min$^{-1}$) as indicated in the respective legends.

S3.2 G band deconvolution for elemental sulfur based 'low S:Fe' fibres

Here we perform peak fitting for the G band in fibres produced using elemental sulfur as the sulfur source.
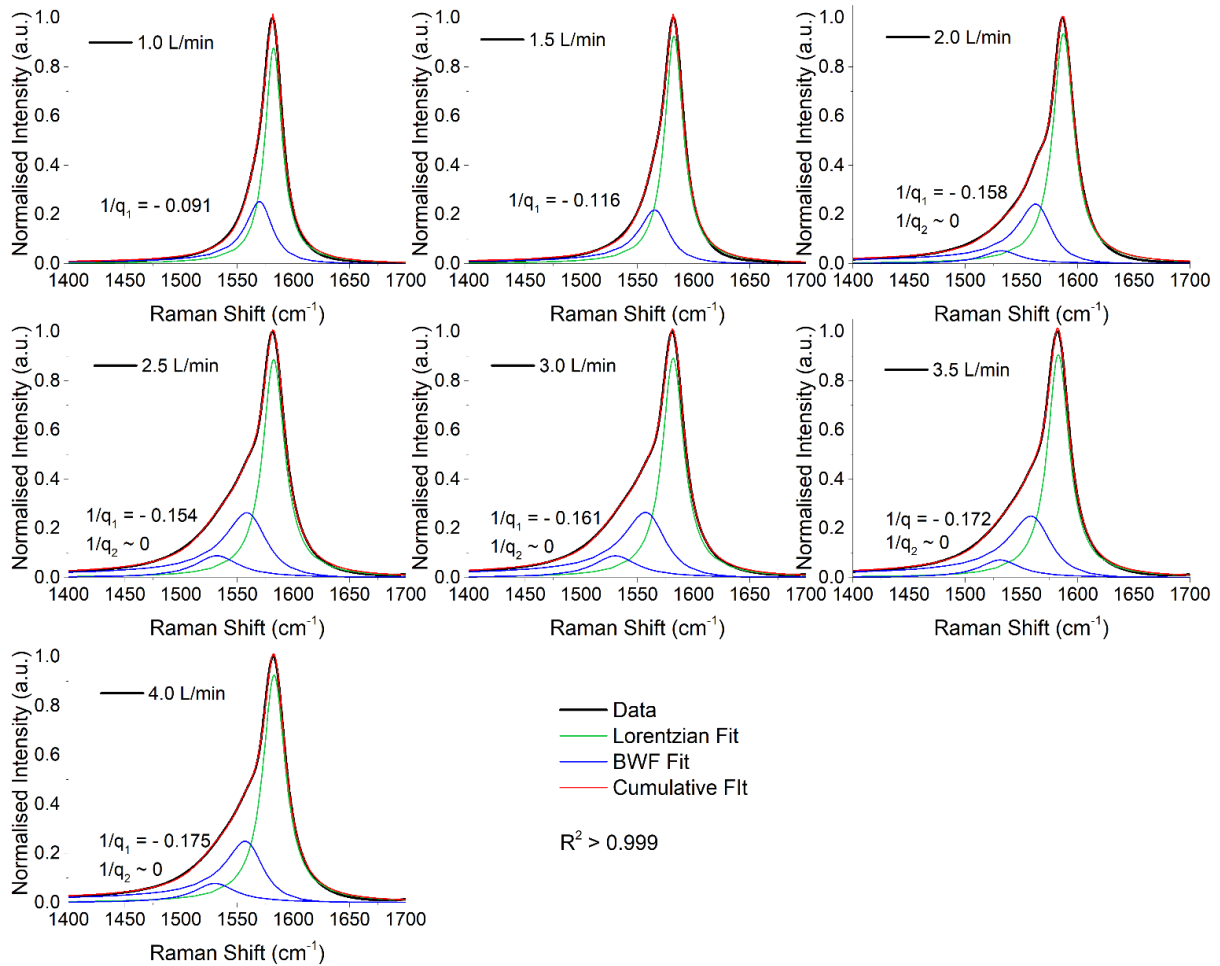


**Figure S13.** Peak fitting to G band (three-peak fit) obtained with $E_L$= 1.58 eV (785 nm) from samples grown at different hydrogen flow rates (as indicated in the respective legends), using elemental sulfur as sulfur source.
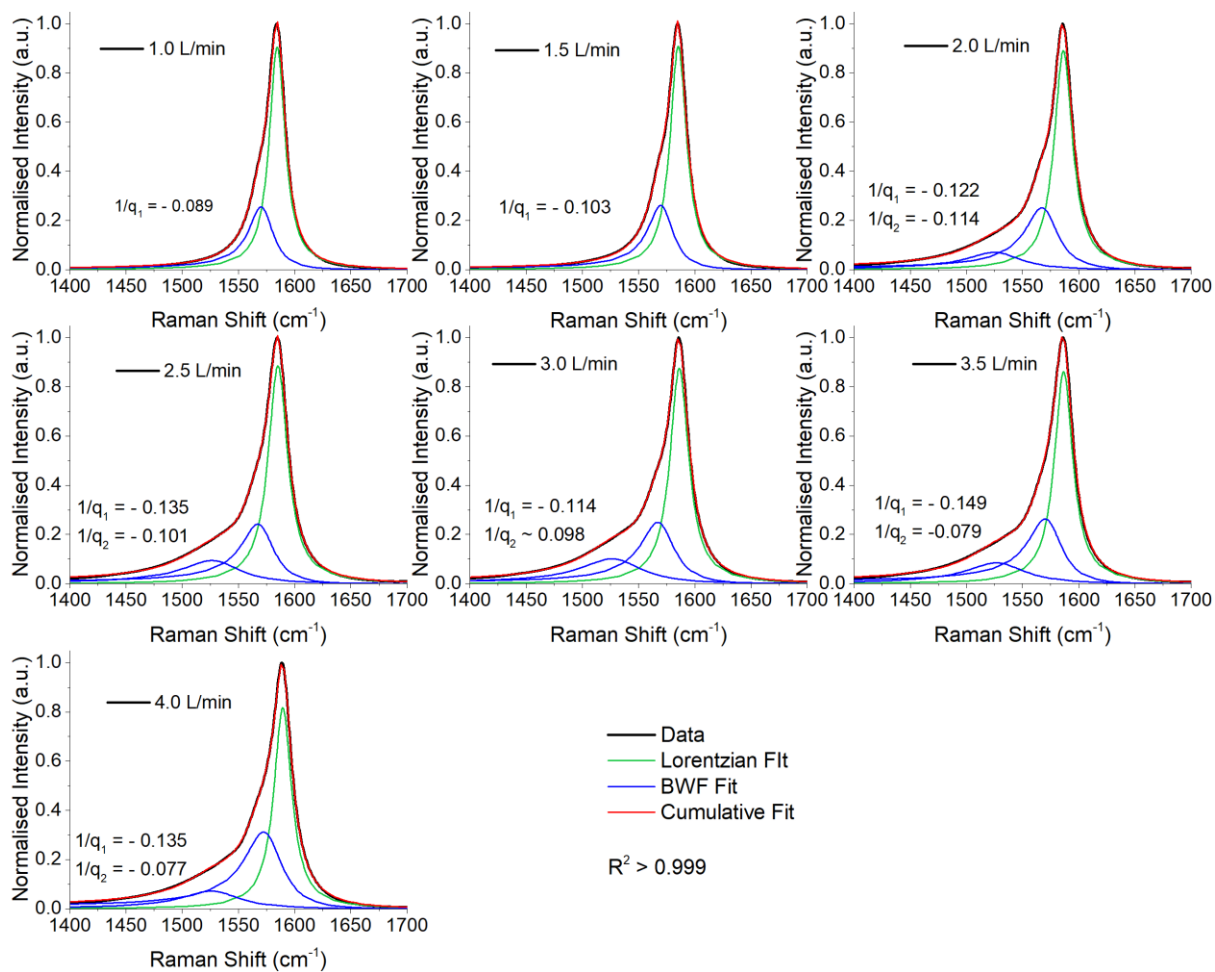
**Figure S14.** Peak fitting to G band obtained with $E_L$= 1.96 eV (633 nm) from samples grown at different hydrogen flow rates (as indicated in the respective legends), using elemental sulfur as sulfur source.
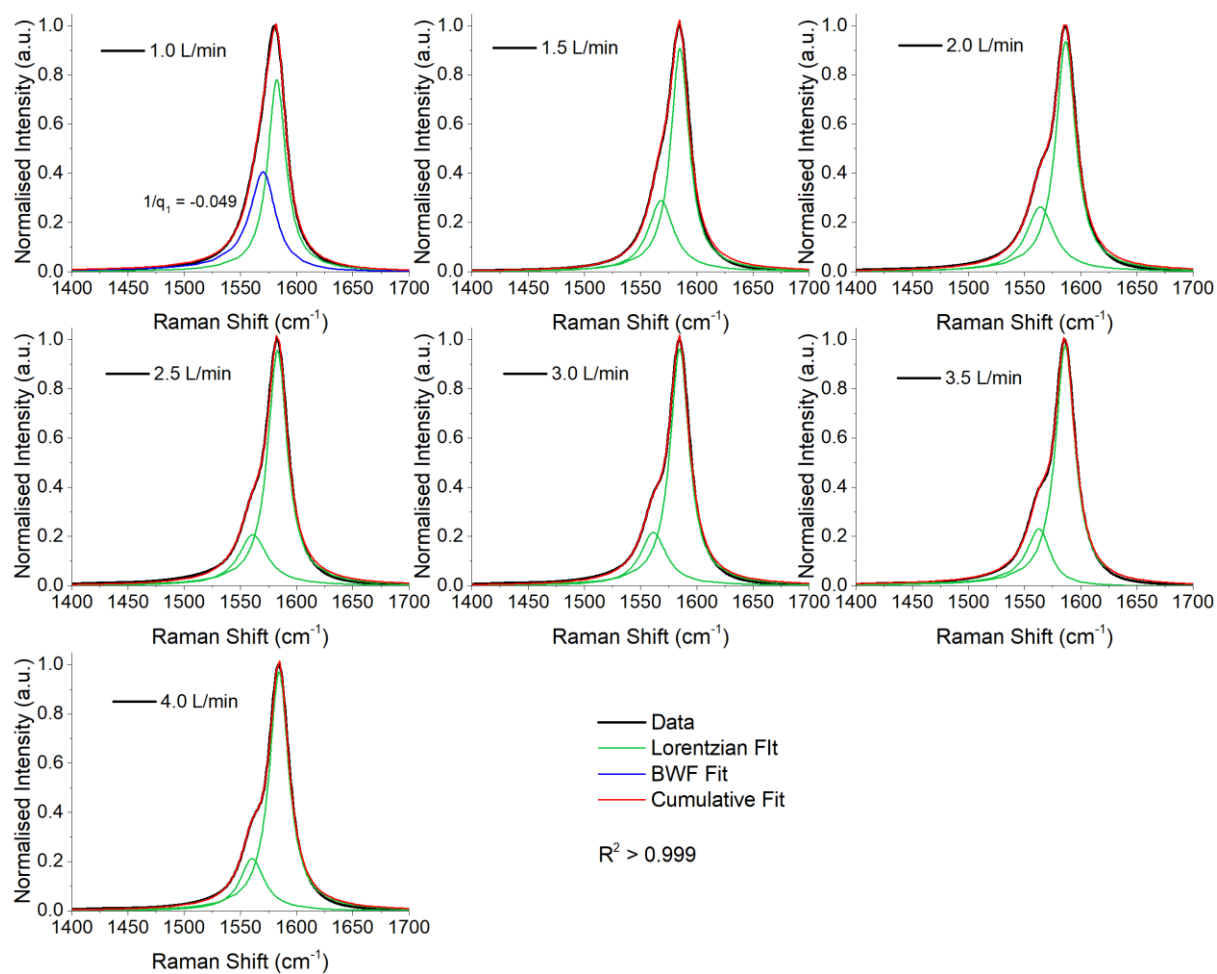
**Figure S15.** Peak fitting to G band obtained with $E_L$= 2.33 eV (532 nm) from samples grown at different hydrogen flow rates (as indicated in the respective legends), using elemental sulfur as sulfur source.

S4. Raman spectra of high S:Fe (1.52) CNT fibres
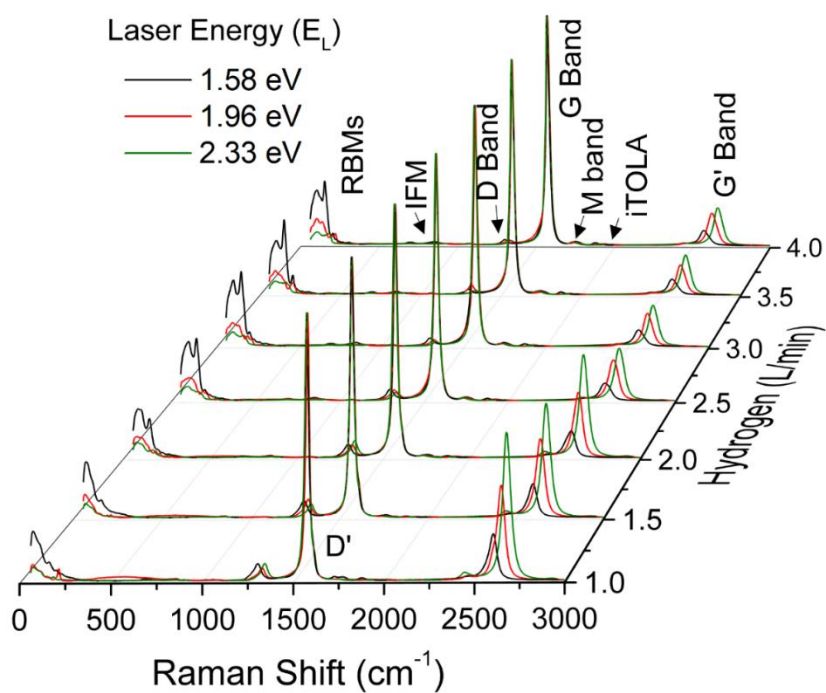


**Figure S16**. Raman spectra of CNT fibres from high-sulfur thiophene recipe.
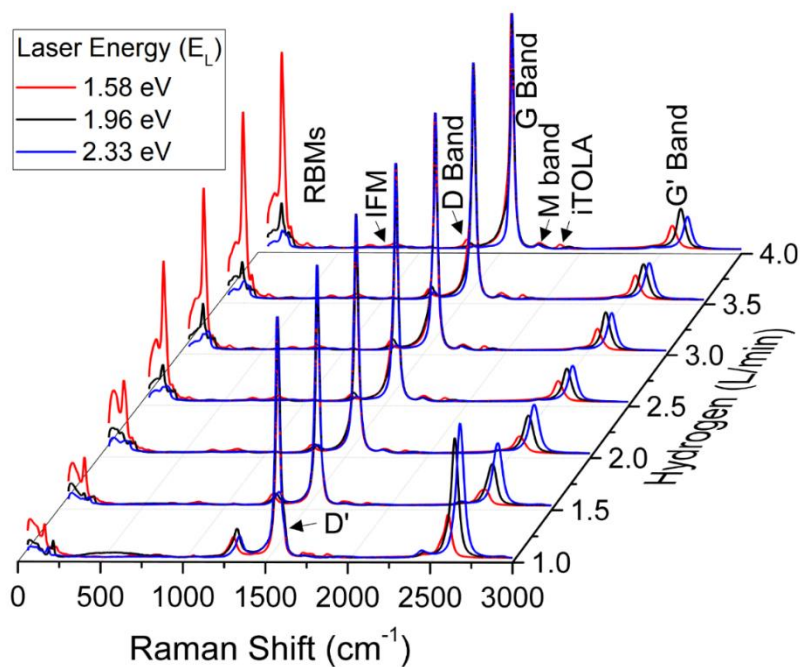


**Figure S17**. Raman spectra of CNT fibres from high-sulfur carbon disulfide recipe.

Comparing Figures S16 (thiophene based) and S17 (carbon disulfide based) with their low S:Fe counterparts in Figure S7, we see that the RBM intensities are lower under high sulfur concentrations. The resonance condition being unchanged, the decrease in RBM intensity shows a suppression of SWCNT growth under high-S low-hydrogen conditions.
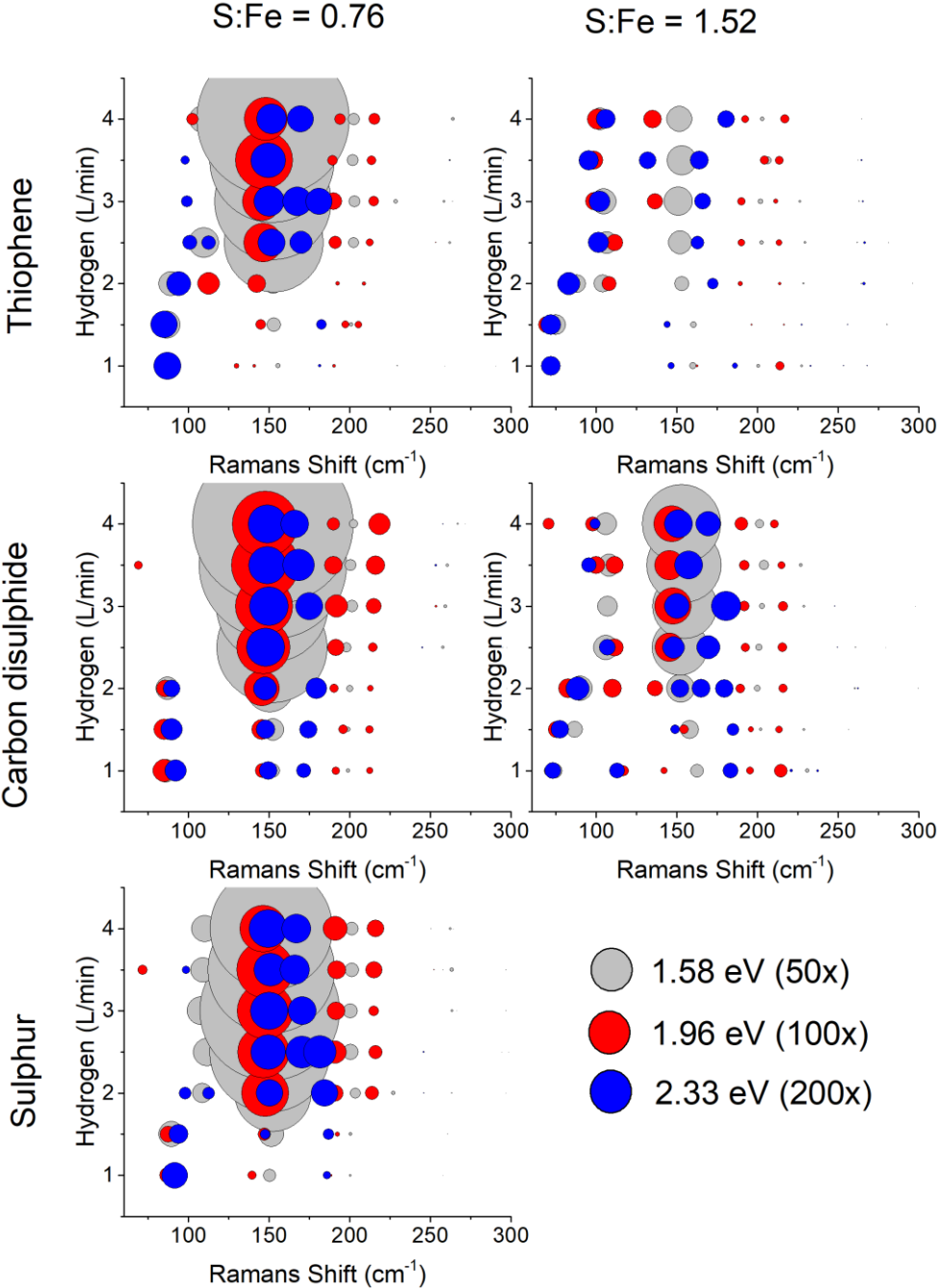


**Figure S18.** A bubble plot of RBMs present in the samples. Colors indicate different laser energies, size indicates normalized intensities, scaled by the indicated multiplication factor for better visibility.

17

The RBM maps identify the various RBMs observed under different laser illuminations. We see that there are peaks at ~ 150 cm$^{-1}$ at all energies, indicating that we have nearly monodisperse diameters rather than similar helicities.

S4.1 G band deconvolution for thiophene based 'high S:Fe' fibres

In the fitting analyses below, notice the occurrence of D' band at low flow rates, and the

lower asymmetry numbers compared to the recipe with lower sulfur concentrations.
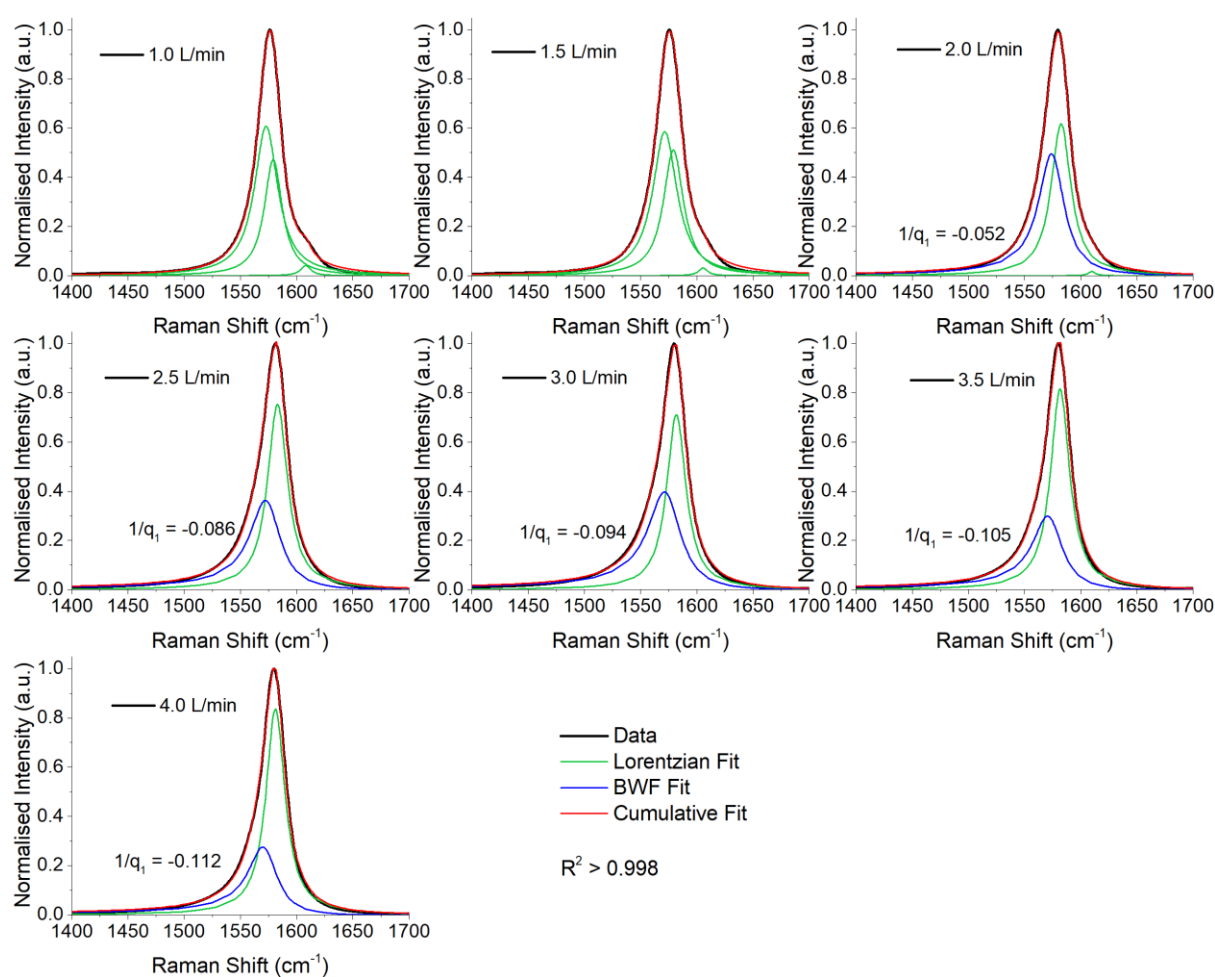


**Figure S19.** Peak fitting to G band (three-peak fit) obtained with $E_L$= 1.58 eV (785 nm) from samples grown at different hydrogen flow rates (as indicated in the respective legends), using thiophene (S:Fe = 1.52) as sulfur source.
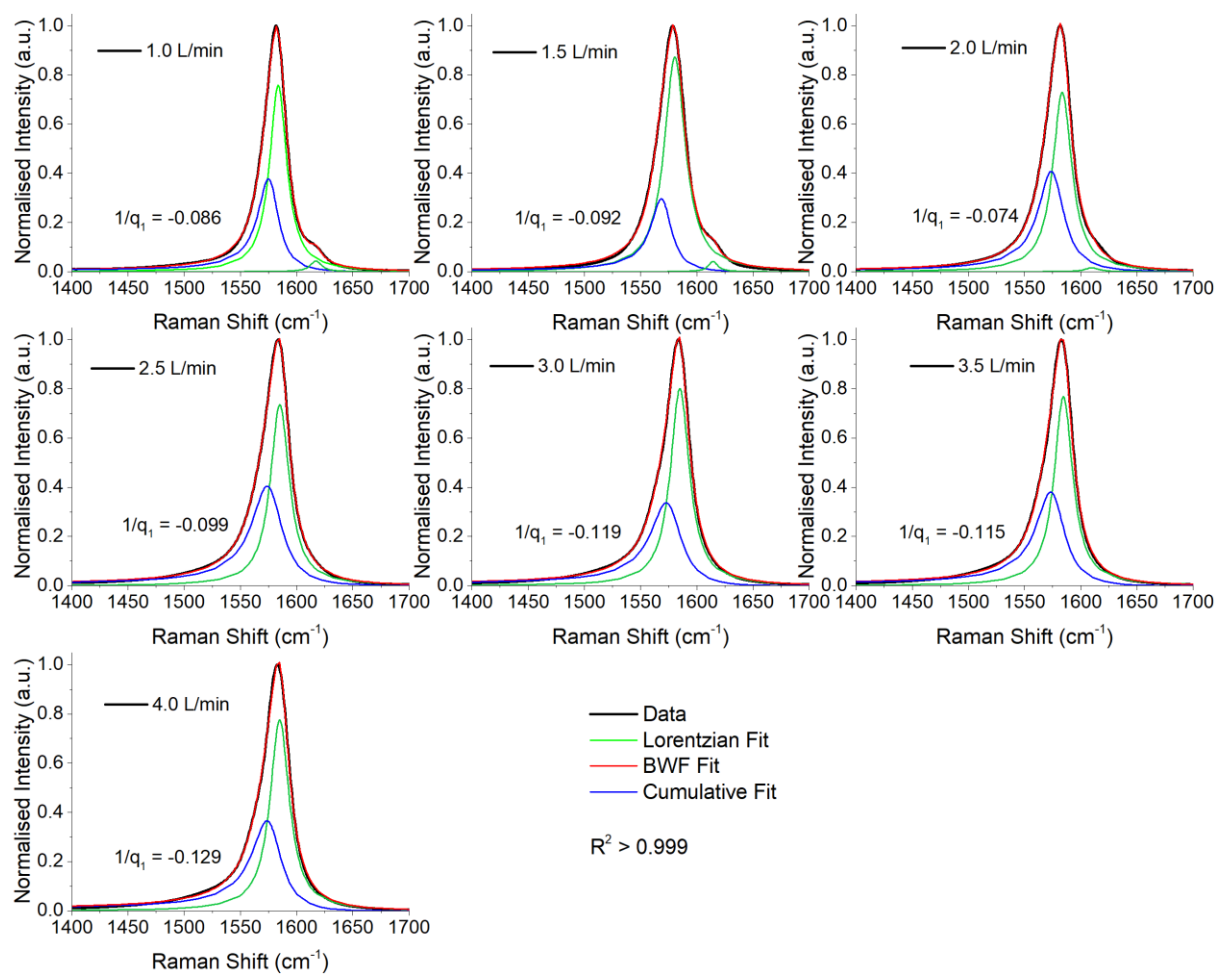
**Figure S20.** Peak fitting to G band obtained with $E_L$= 1.96 eV (633 nm) from samples grown at different hydrogen flow rates (as indicated in the respective legends), using thiophene (S:Fe = 1.52) as sulfur source.
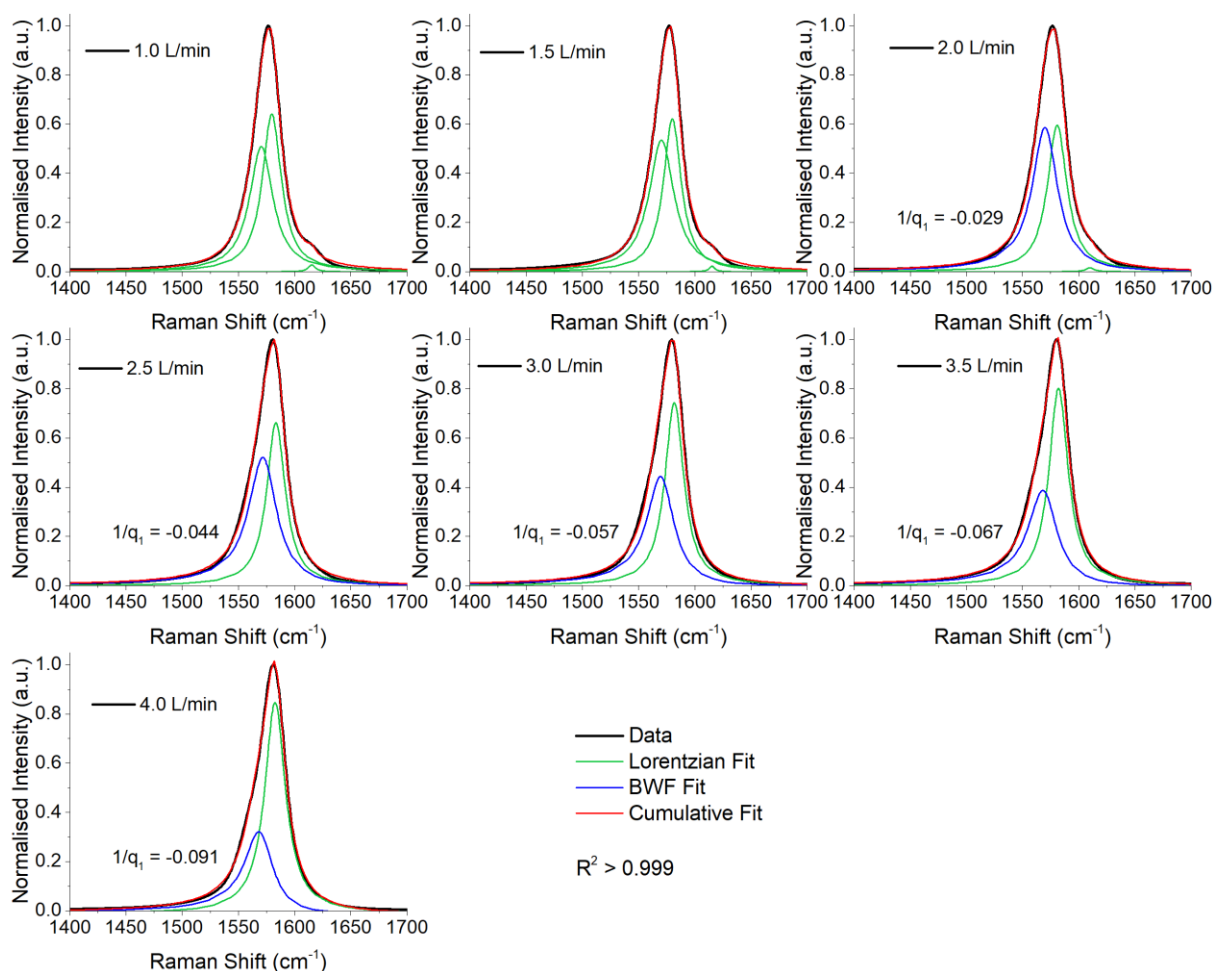
**Figure S21.** Peak fitting to G band obtained with $E_L$= 2.33 eV (532 nm) from samples grown at different hydrogen flow rates (as indicated in the respective legends), using thiophene (S:Fe = 1.52) as sulfur source.

Thus, the asymmetry factor for the G⁻ bands in Figures S19-21 are lower than their low S:Fe counterparts in Figures S3-S5. A lower asymmetry suggests a lower proportion of small diameter nanotubes are produced under high sulfur conditions. Interestingly, at low-hydrogen flow rates at high sulfur concentration, an additional D' band can be fit on the high wavenumber side of the G band. This band is indicative of defective tubes or MWCNTs. Although the presence of the D' band also has the effect of making the G band appear asymmetric, the discussion of asymmetry in G band is usually limited to the constituents of the G band.

## S4.2 G band deconvolution for carbon disulfide based 'high S:Fe' fibres
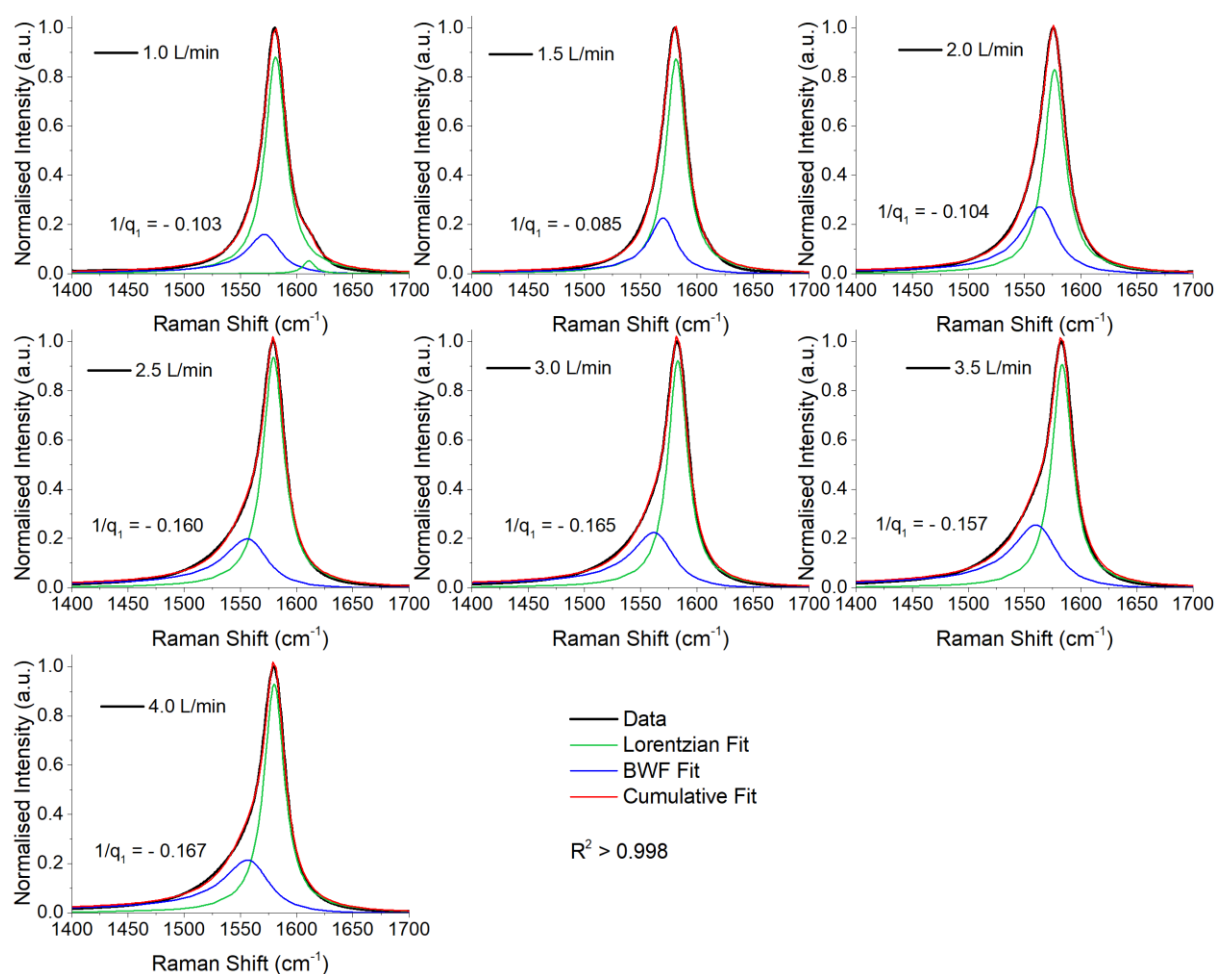


**Figure S22.** Peak fitting to G band (three-peak fit) obtained with $E_L$= 1.58 eV (785 nm) from samples grown at different hydrogen flow rates (as indicated in the respective legends), using carbon disulfide (S:Fe = 1.52) as sulfur source.
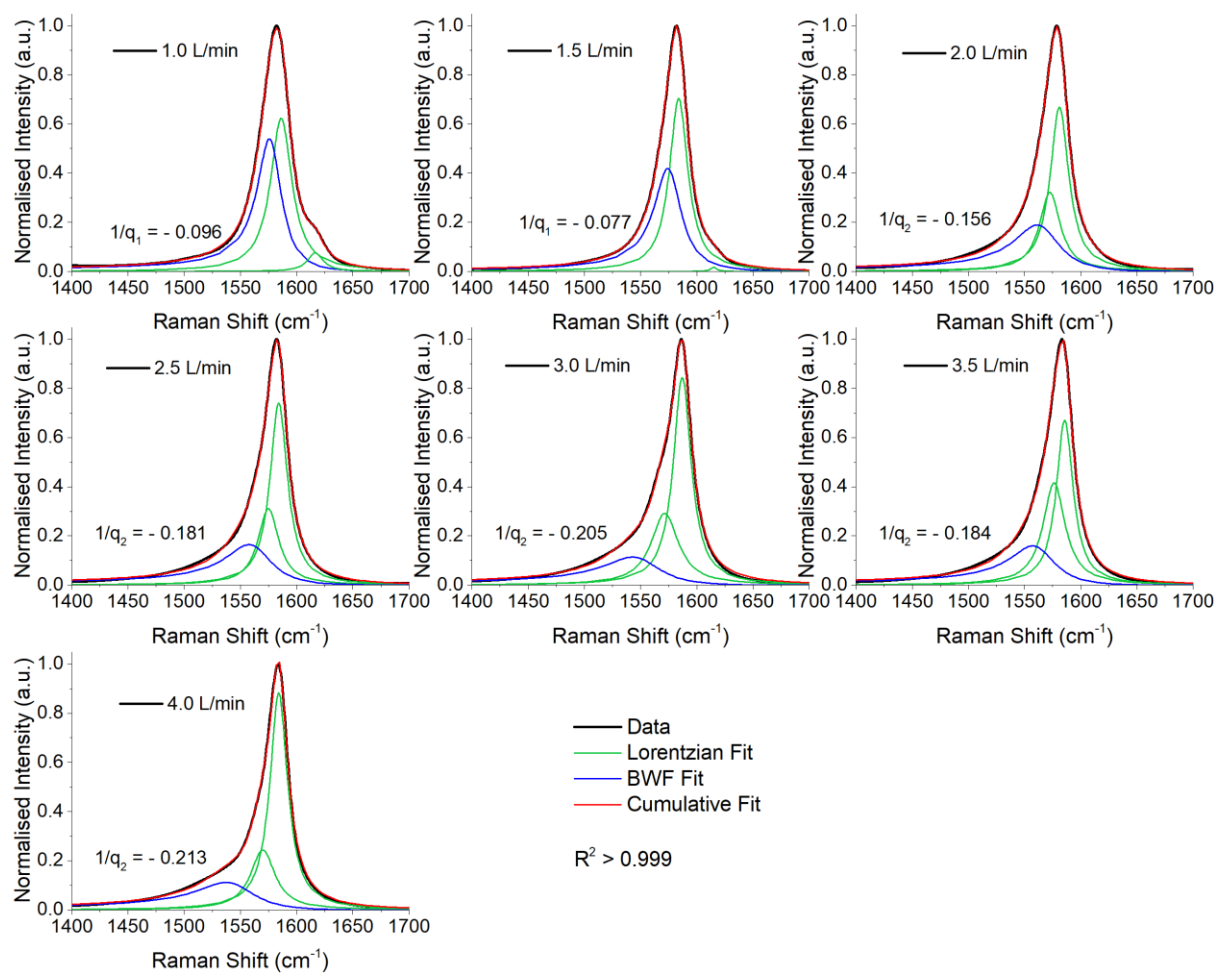
**Figure S23.** Peak fitting to G band obtained with $E_L$ = 1.96 eV (633 nm) from samples grown at different hydrogen flow rates (as indicated in the respective legends), using carbon disulfide (S:Fe = 1.52) as sulfur source.
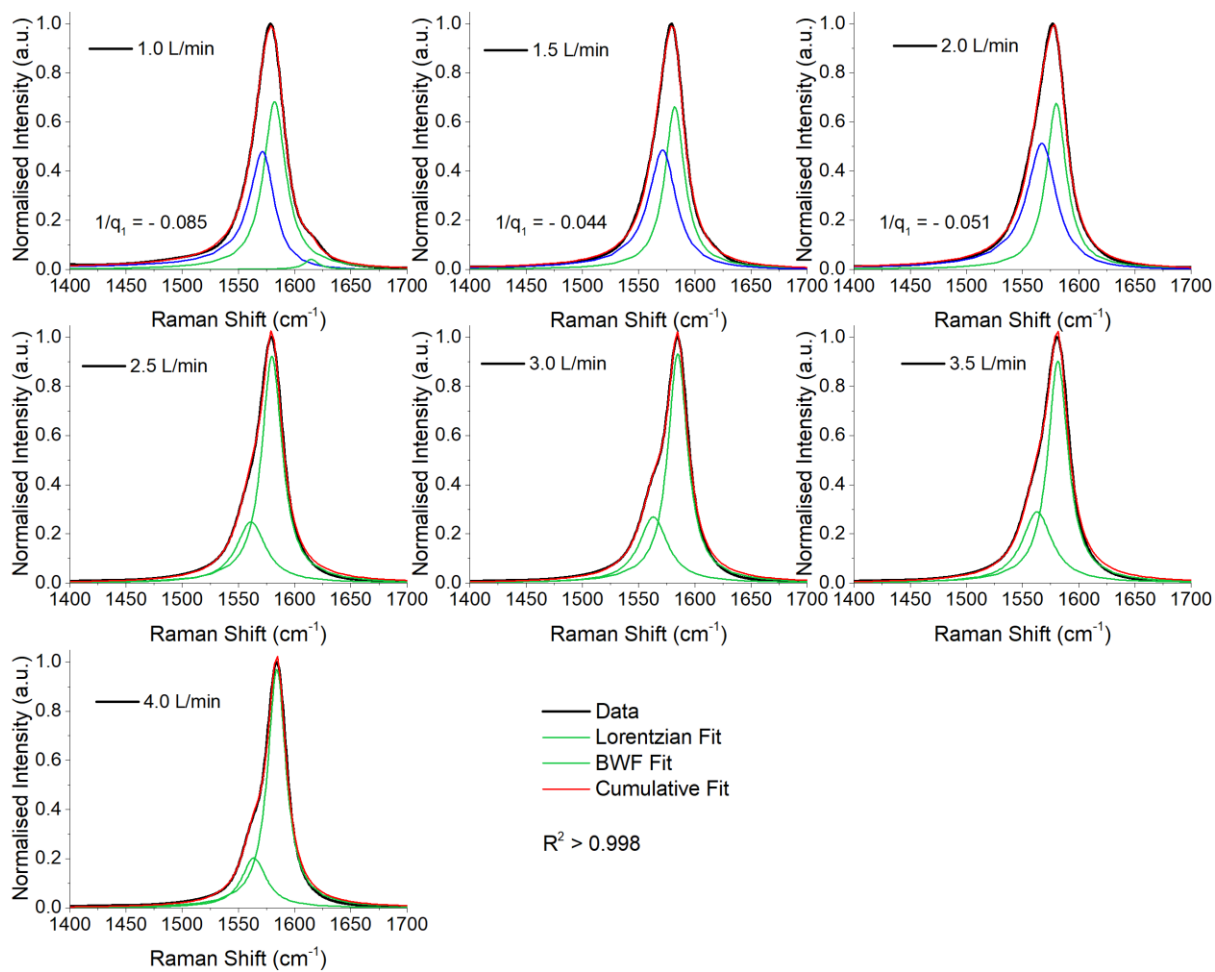
**Figure S24.** Peak fitting to G band obtained with $E_L$= 2.33 eV (532 nm) from samples grown at different hydrogen flow rates (as indicated in the respective legends), using carbon disulfide (S:Fe = 1.52) as sulfur source.

S5. Thermogravimetric analyses
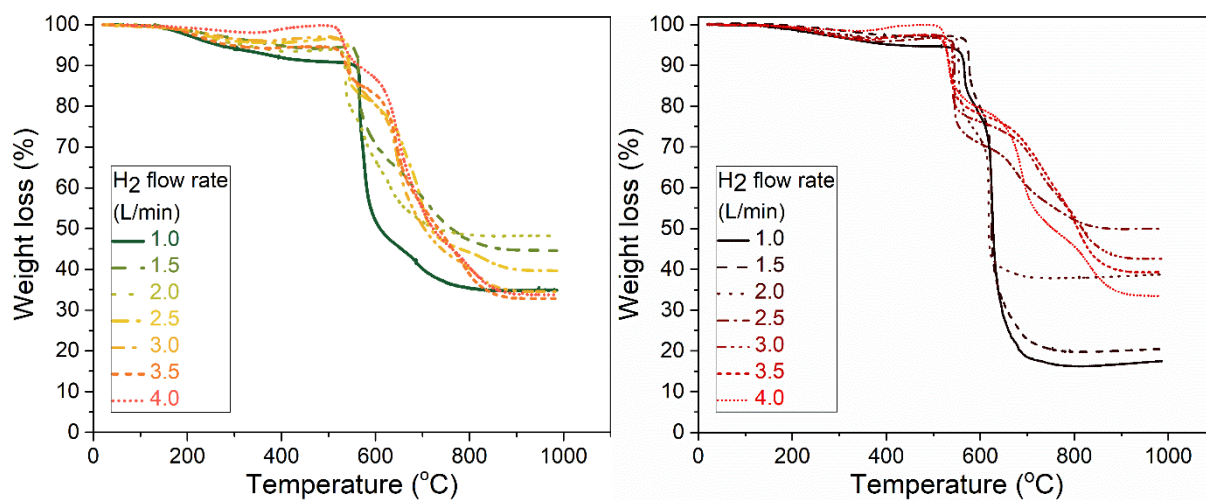


**Figure S25.** (a) TGA mass loss curves of samples spun using thiophene as sulfur source at sulfur concentrations of (left) S:Fe = 0.76, and (right) S:Fe = 1.52. These corresponding to the derivative curves shown in Figure 4a and 4b (see main text), respectively.

As discussed in the main text, high-sulfur recipes produce less amorphous carbon (a-C) than low-sulfur recipes. Since the high-sulfur recipes also favour MWCNT production, this suggests that more carbon is utilized by the catalyst particles under these conditions, thus making less non graphitised carbon.

S6. Material Yields
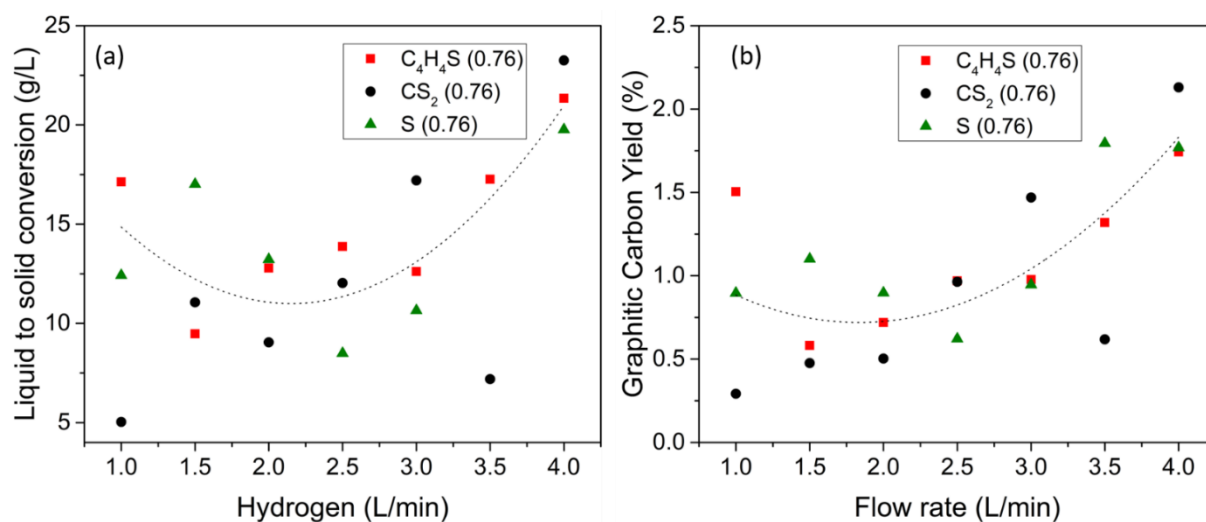


**Figure S26.** (a) Amount of total mass collected per unit of liquid injected, and (b) percentage of graphitic carbon in the samples. The dotted lines are included as a guide to the eye for the behaviour of the combined data sets, and the minima correspond to regions where spinning is difficult.


## S7. Electron microscopy

In this section, we provide Scanning and Transmission electron microscopy (SEM and TEM) images of samples spun at different conditions.

In the SEM images, we see that sample consist of fibre bundles, with varying amounts of amorphous carbon and residual catalyst. The residual catalyst amount varies in same fashion as observed via TGA, i.e. peeking in amount at an intermediate flow rate.

We have provided EM images of samples grown at hydrogen flows of 1 and 4 L min-1 at different magnifications and locations. In general, low hydrogen samples have a broad distribution in tube diameters, there are collapsed tubes, large diameter single-wall tubes and large Fe catalyst particles. In high hydrogen samples, there are smaller tubes and catalyst particles.
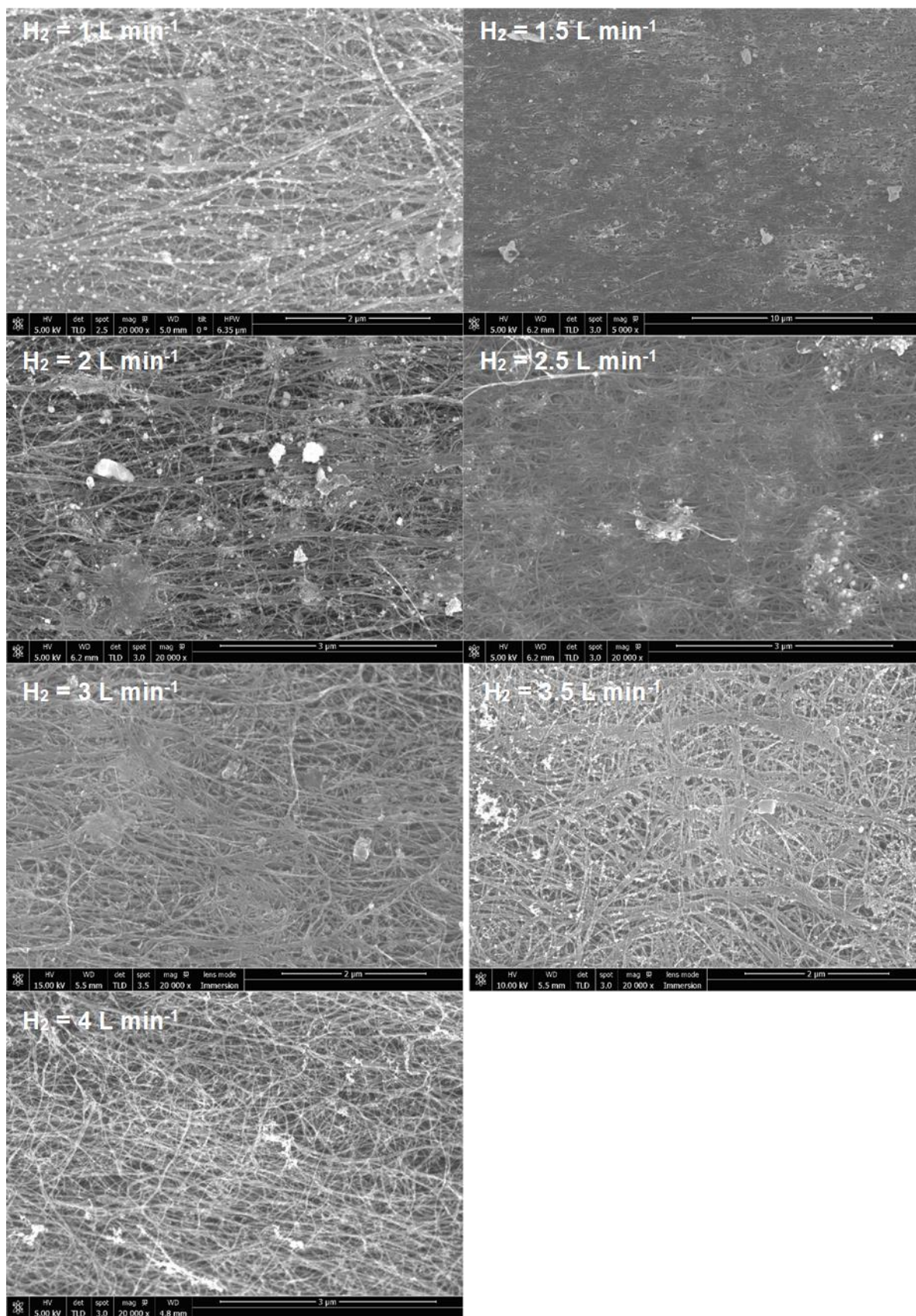
**Figure S27.** SEM images of CNT fibres produced at different flow rates (as indicated in the legends) with thiophene as the sulfur source at S:Fe = 0.76.
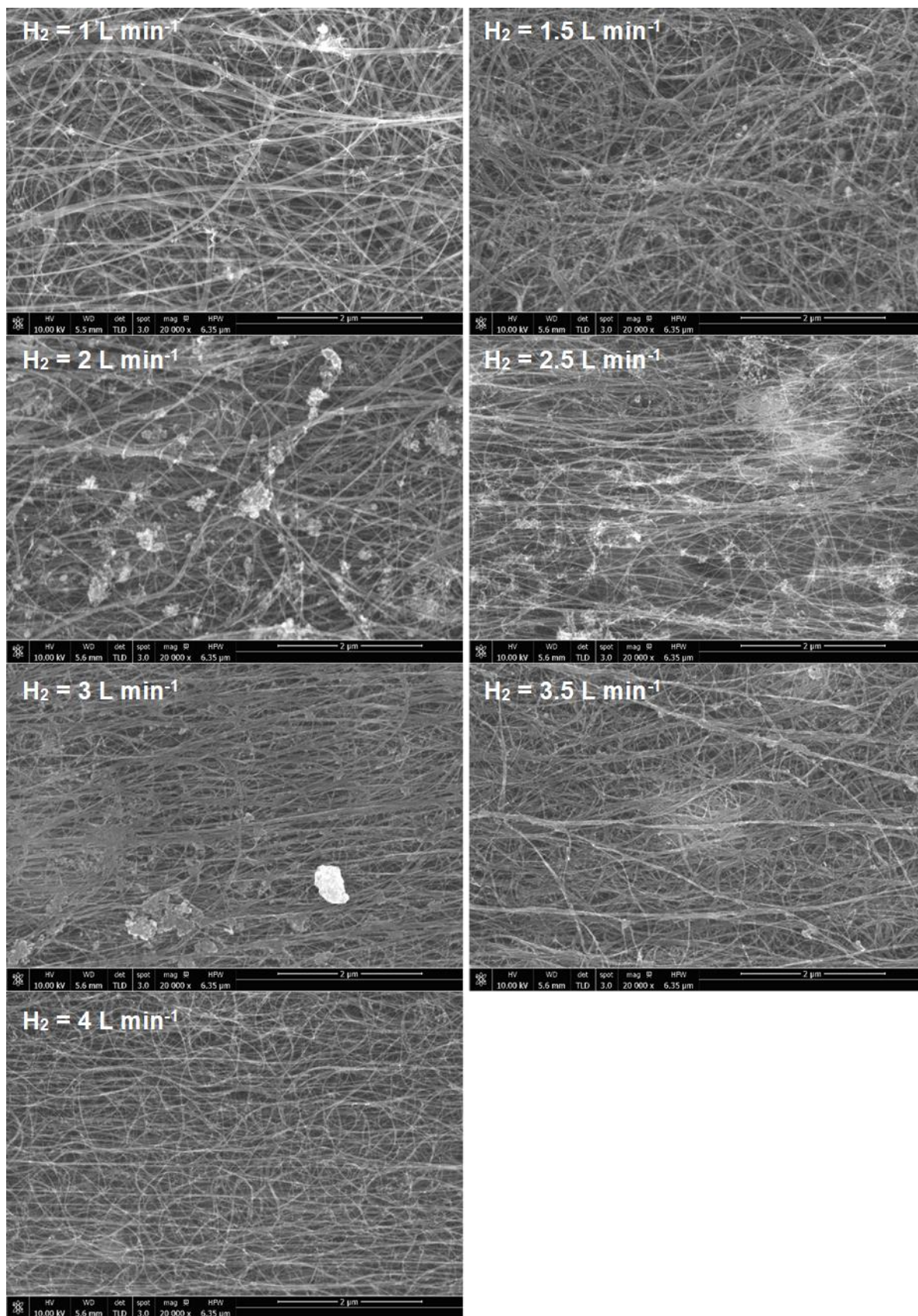
**Figure S28.** SEM images of CNT fibres produced at different flow rates (as indicated in the legends) with thiophene as the sulfur source at S:Fe = 1.52.
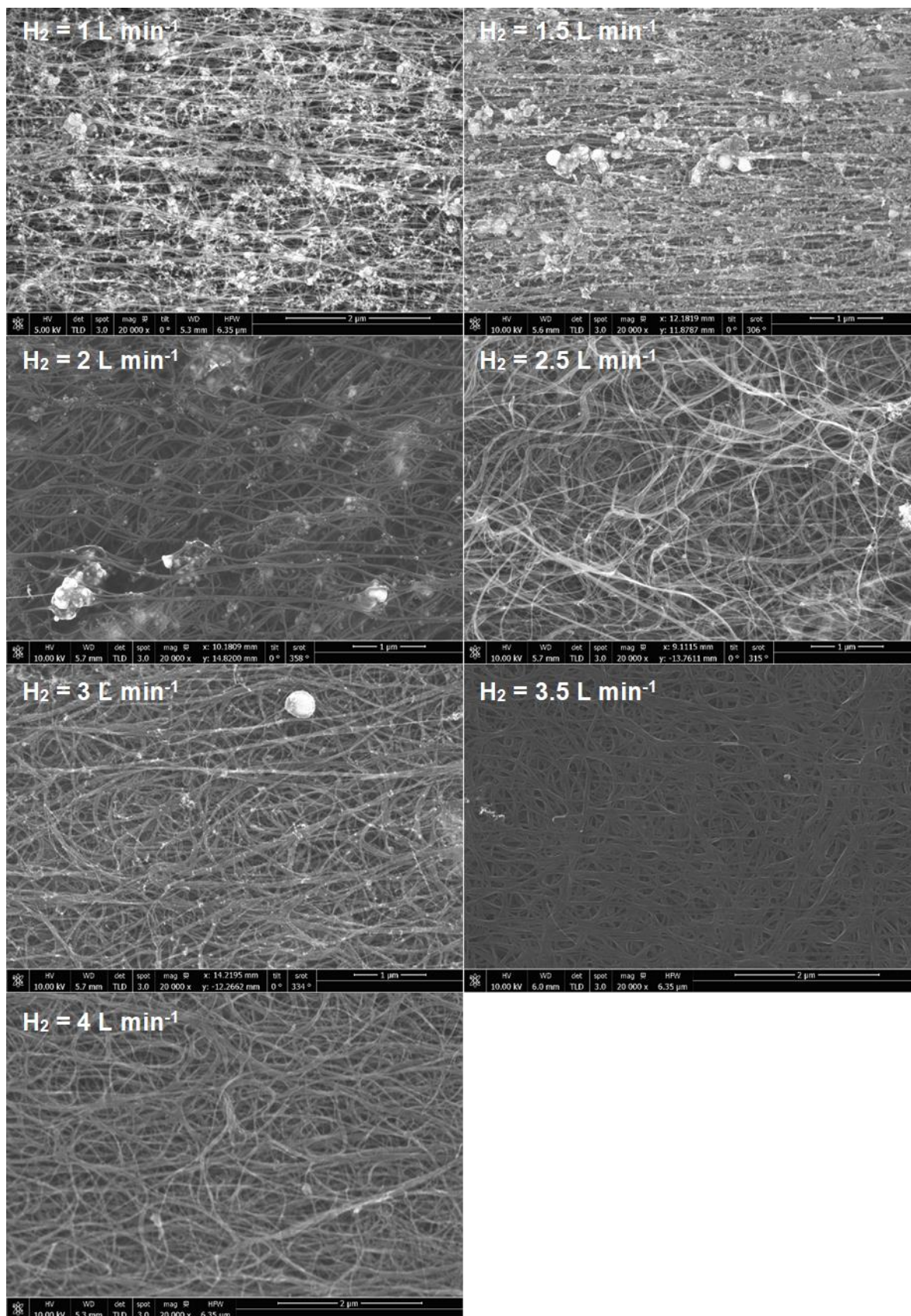
**Figure S29.** SEM images of CNT fibres produced at different flow rates (as indicated in the legends) with carbon disulfide as the sulfur source at S:Fe = 0.76.
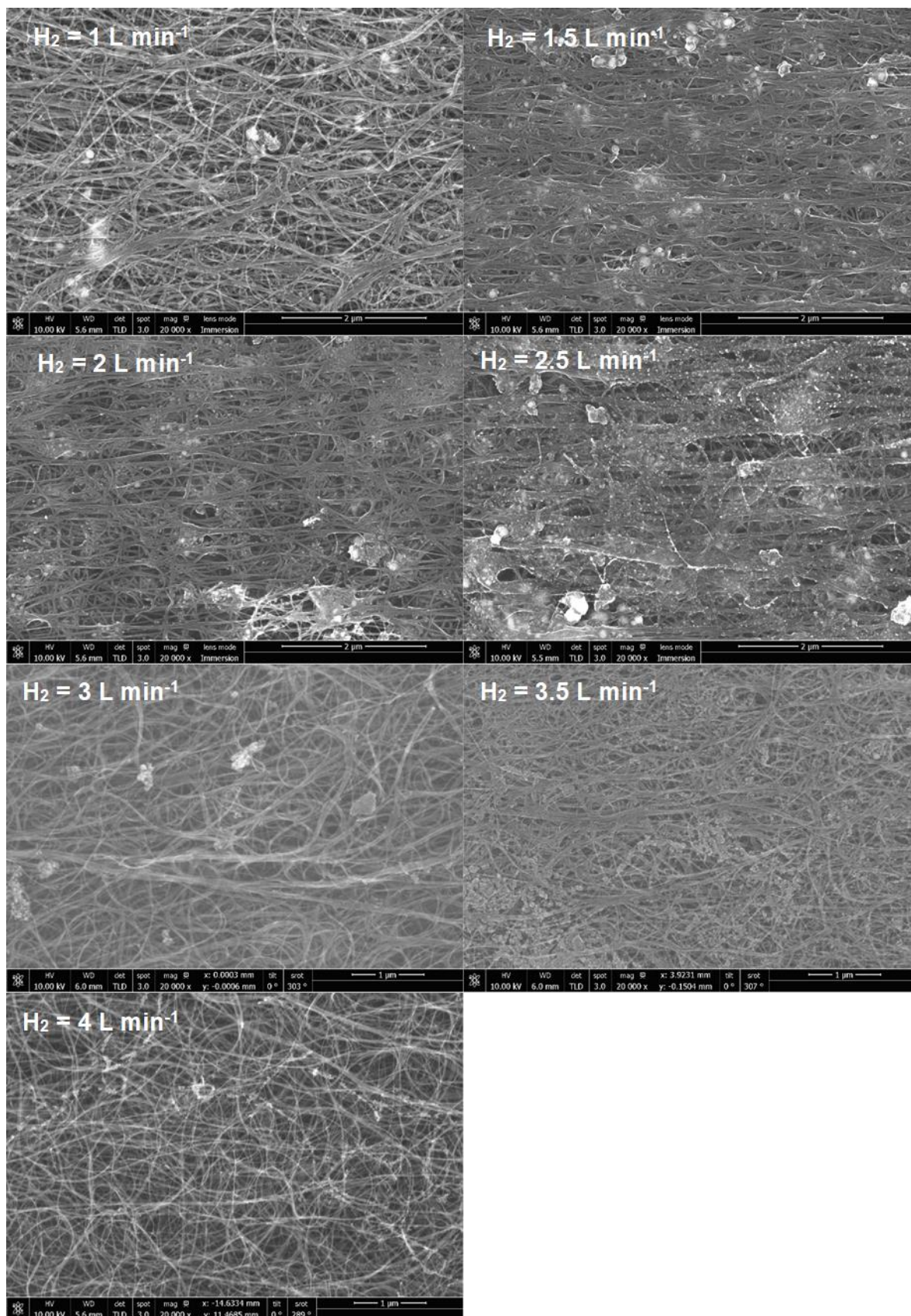
**Figure S30.** SEM images of CNT fibres produced at different flow rates (as indicated in the legends) with carbon disulphide as the sulfur source at S:Fe = 1.52.
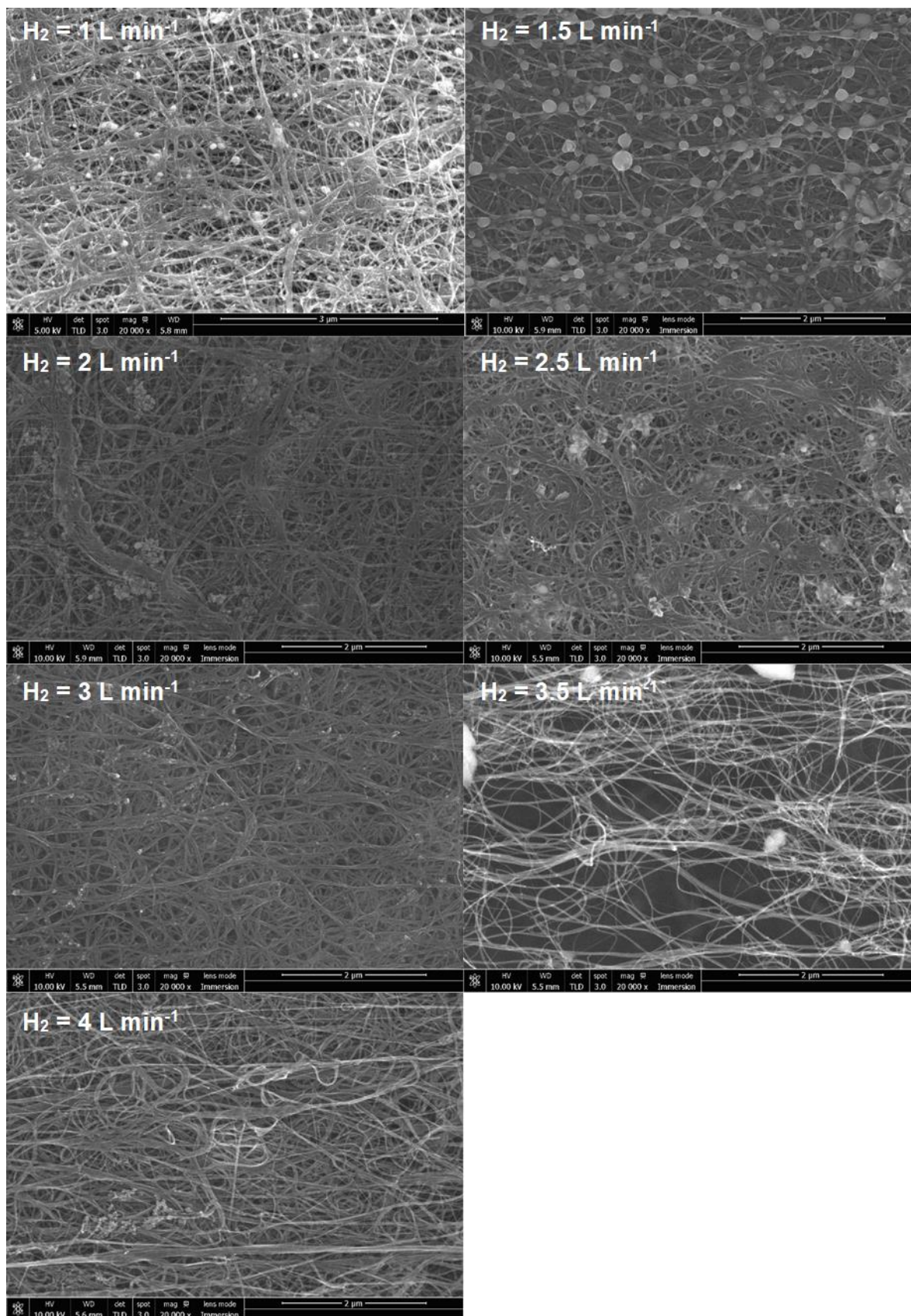
**Figure S31.** SEM images of CNT fibres produced at different flow rates (as indicated in the legends) with elemental sulfur as the sulfur source at S:Fe = 0.76.
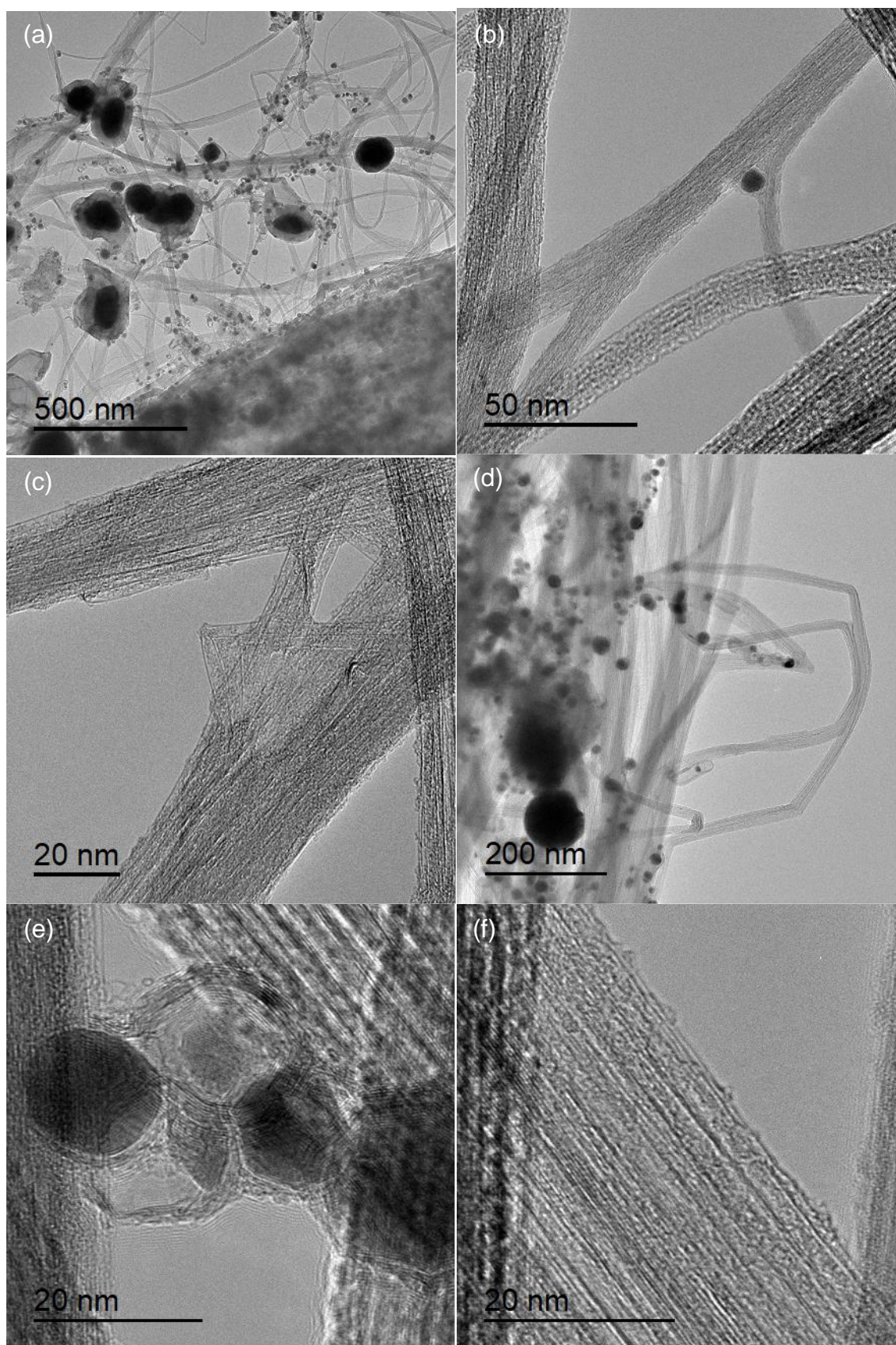
**Figure S32.** TEM images of CNT fibres produced at H$_2$ flow of 1 L min$^{-1}$ with thiophene as the sulfur source at S:Fe = 0.76: (a-c) as-is fibre, (d-f) surfactant dispersed fibres.
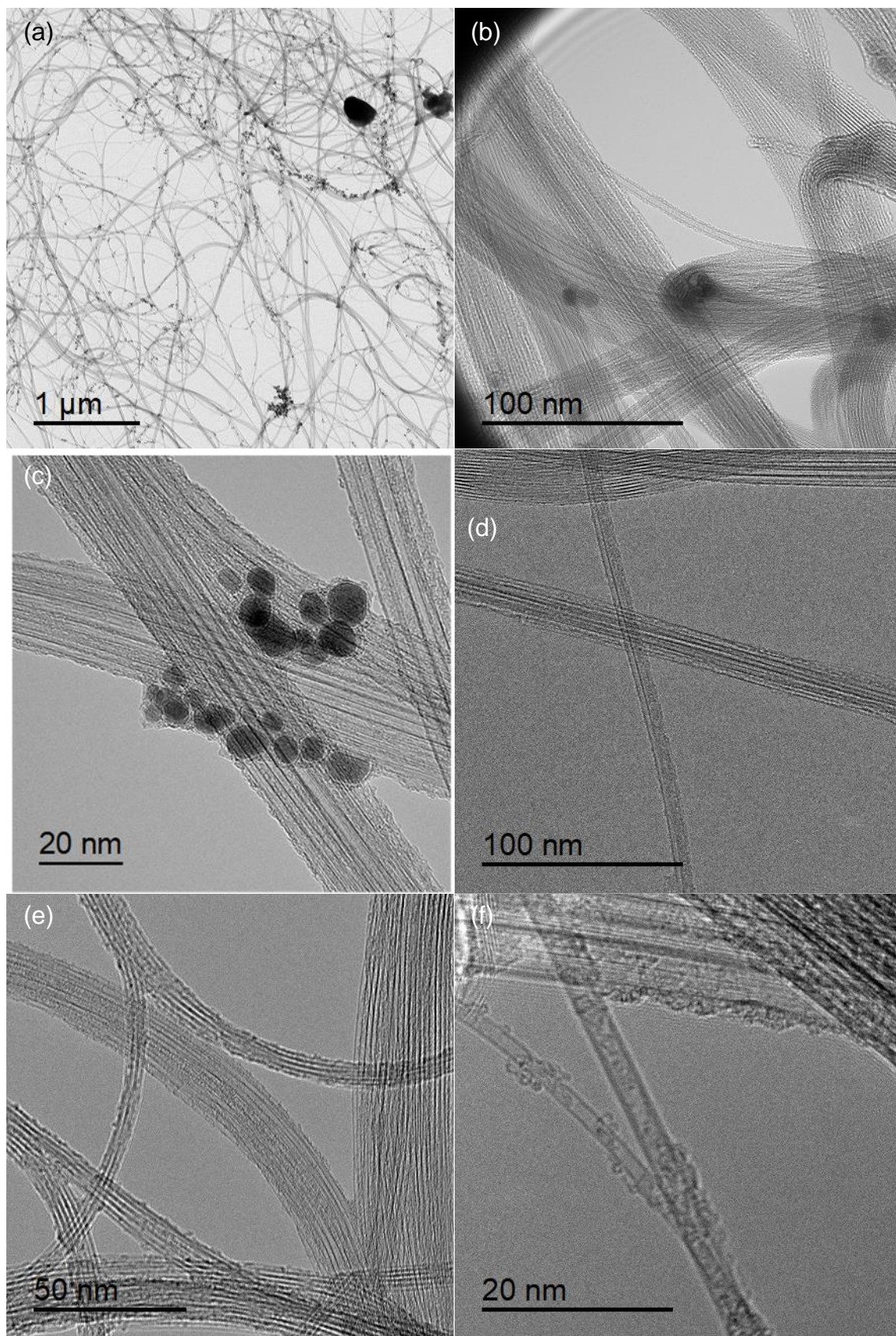
**Figure S33.** TEM images of CNT fibres produced at H$_2$ flow of 4 L min$^{-1}$ with thiophene as the sulfur source at S:Fe = 0.76: (a-c) as-is fibre, (d-f) surfactant dispersed fibres.
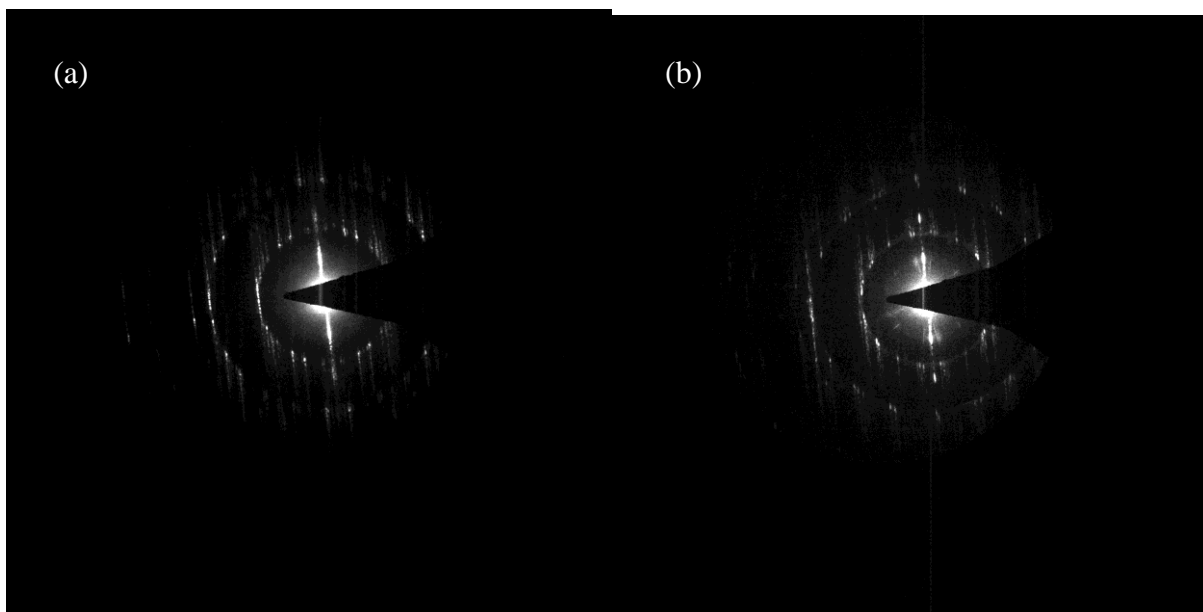
**Figure S34.** Electron diffraction patterns from random CNTs in a "low-hydrogen" sample.
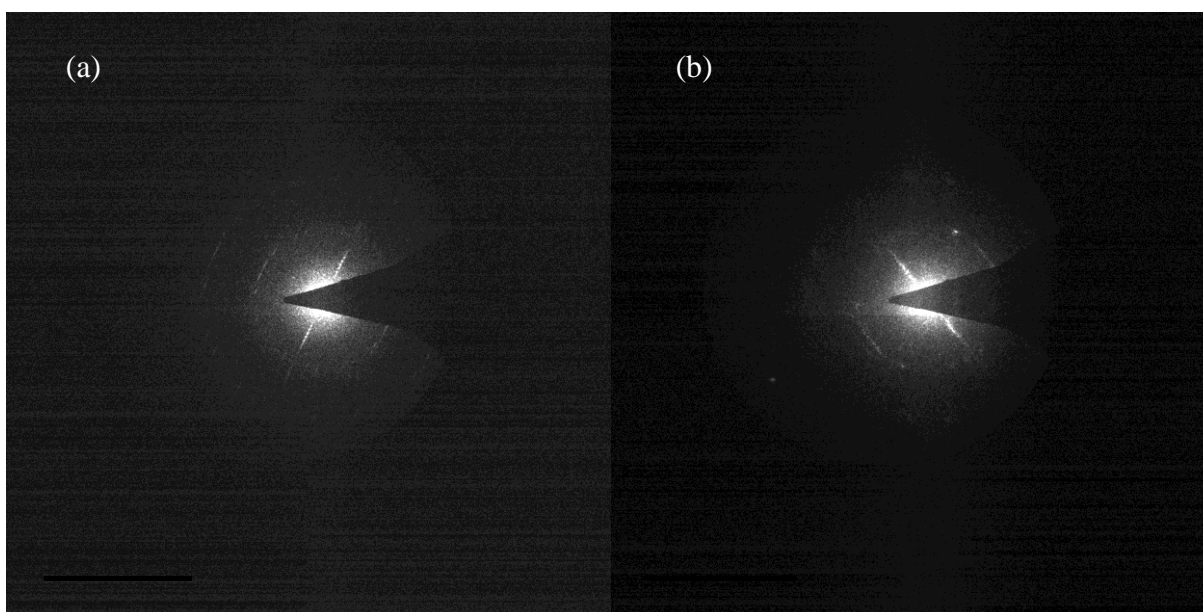


**Figure S35.** Electron diffraction patterns from random CNTs in a "high-hydrogen" sample.

The electron diffraction data while not statistically relevant enough to make sweeping claims of nanotube helicities, it appears that the "low-hydrogen" (Figures S34(a) and (b)) samples are dominated by few to multi-wall CNTs. MWCNTs are characterised by multiple peaks in the equatorial lines and several pairs of principles lines. In SWNTs, one equatorial line with three main principal lines are expected. In SWCNT bundles, the principal lines smear to give an arc like appearance, as can be seen from randomly selected regions in a "high-hydrogen" sample in figures S35 (a) and (b).

## S8. Process validation

**Table S2.** Raman (1.58 eV) G:D ratios of samples produced in the horizontal reactor.

| $H_2$ flow (L/min) | G:D (S:Fe=0.76) | G:D (S:Fe=1.52) |
|---|---|---|
| 1.0 | 14.4 | 10.8 |
| 1.5 | 10.0 | N/A |
| 2.0 | 24.1 | 8.0 |
| 3.0 | 29.2 | 5.8 |
| 4.0 | 71.0 | 20.3 |
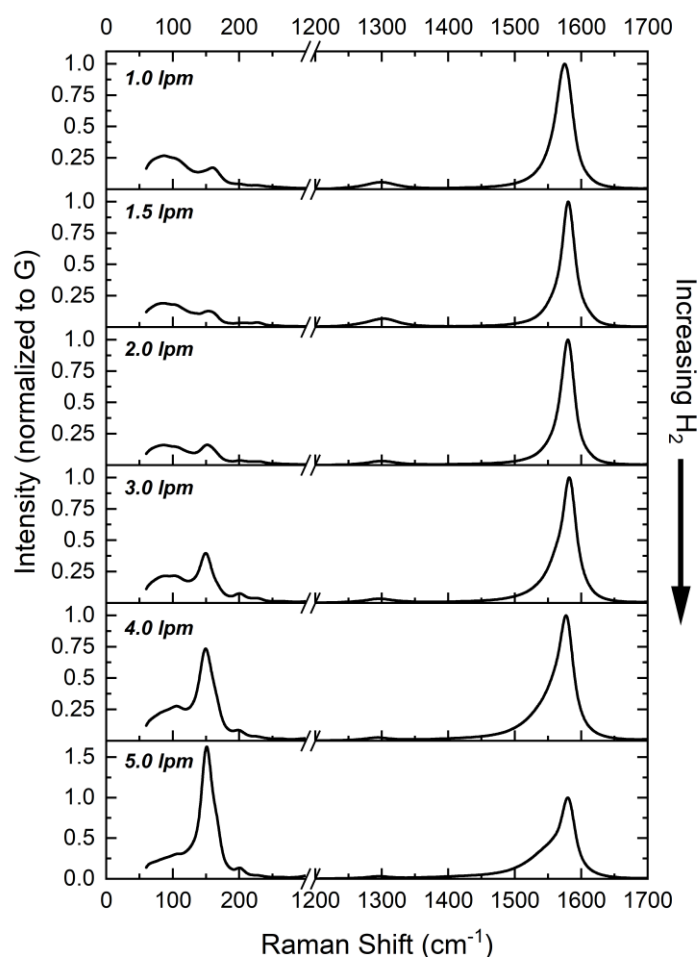


**Figure S36**. Raman (1.58 eV) spectra of materials produced in the horizontal reactor from the low sulfur (S:Fe = 0.76) thiophene-based solution at different $H_2$ flow rates (as indicated in the legends). The data are normalized to the intensity of the G band. 'lpm' stands for litre per minute.
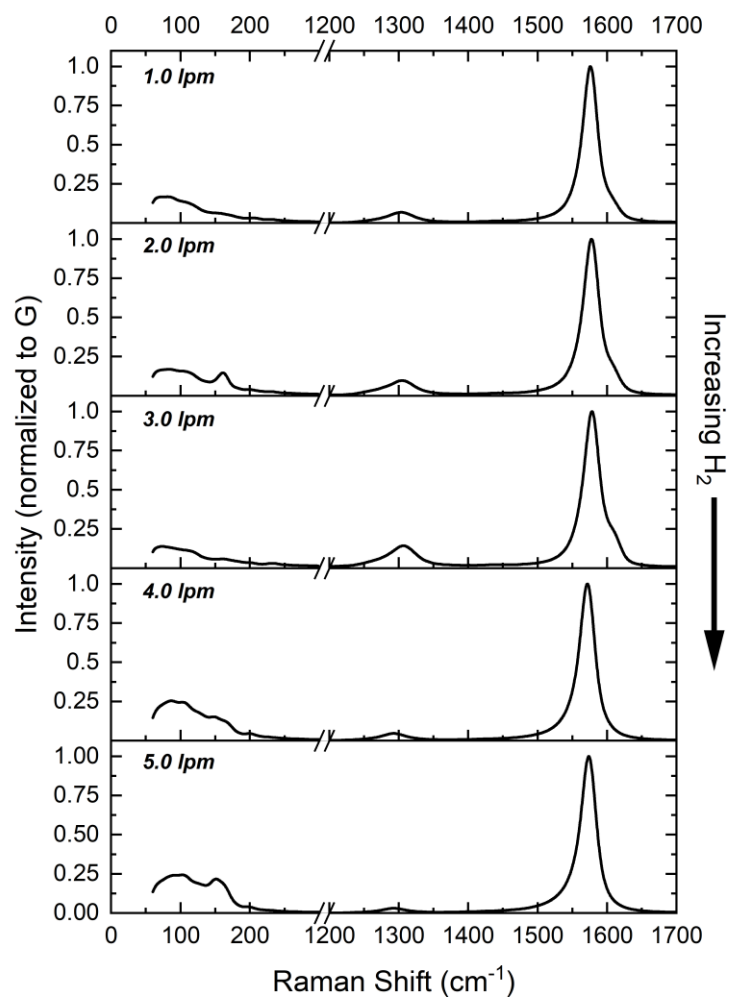
**Figure S37.** Raman (1.58 eV) spectra of materials produced in the horizontal reactor from the high sulfur (S:Fe = 1.52) thiophene-based solution at different $H_2$ flow rates (as indicated in the legends). The data are normalized to the intensity of the G band. 'lpm' stands for litre per minute.